Shock Wave Emission by Laser Generated Bubbles

Werner Lauterborn and Alfred Vogel

Abstract. The phenomena occurring when short pulses of laser light are focused into a liquid are reviewed from the first findings after the invention of the laser to the present state of knowledge. Dielectric breakdown with plasma and bubble formation, the breakdown shock wave, bubble dynamics with expansion and collapse, and the bubble collapse shock wave or waves are addressed. Breakdown plasma lengths as a function of laser pulse energy are given. The propagation speed of the breakdown shock wave and the related shock peak pressure as determined by high speed streak recordings for nano-, pico-, and femtosecond laser pulses focused into water are discussed. Breakdown shock wave velocities up to 5000 m/s and peak pressures up to 100 kbar are reported for these monopolar acoustic pulses for laser pulse energies up to some 10 mJ. In tissue bipolar pressure pulses are observed due to the elasticity of the medium. The widths of the shock waves reach values in the range of tens of nano seconds to beyond 100 ns. The simultaneously generated breakdown bubble gets about half of the energy of the shock wave. Bubble energy rises linearly with the laser pulse energy with different slopes depending on the laser pulse duration. Equations for bubble dynamics are given and compared with laser induced bubble dynamics. Strength and width of bubble collapse shock waves measured with PVDF and fiber optic hydrophones are presented together with the breakdown shock waves. Similar values are obtained for both collapse and breakdown in the bulk of the liquid. Shock wave emission from bubbles collapsing near boundaries (solid and elastic) is discussed together with applications in cleaning and erosion or cell destruction.

Werner Lauterborn
Georg-August-Universität Göttingen, Drittes Physikalisches Institut, Göttingen, Germany
e-mail: W.Lauterborn@dpi.physik.uni-goettingen.de

Alfred Vogel
University of Lübeck, Institute of Biomedical Optics, Lübeck, Germany
e-mail: vogel@bmo.uni-luebeck.de

C.F. Delale (Ed.): *Bubble Dynamics & Shock Waves*, SHOCKWAVES 8, pp. 67–103.
DOI: 10.1007/978-3-642-34297-4_3

1 Introduction

Soon after the invention of the laser the interaction of its coherent light with matter attracted the attention of many a researcher. At first, mainly the propagation of laser light through gases and (transparent) solids was investigated to study nonlinear electromagnetic wave propagation and wave interaction. Thereby, for instance, second harmonic generation, now abundently used, came into being. Investigations of laser light interaction with liquids were rare at that time. Only comparably few articles appeared in the 1960s covering the aspect of focused laser light in liquids, the topic of the present chapter. In a time span of ten years after the first report in 1963 [1] about one article only appeared per year [1, 2, 3, 4, 5, 6, 7, 8, 9, 10]. The first experiments started with Q-switched ruby laser pulses (wavelength 694.3 nm, pulse width about 30 ns, energy per pulse about 0.01 to 0.2 J [3, 5], focal beam diameter in the order of 35 μm [4]) focused into water and some other liquids. However, other wavelengths (1.06 μm from a neodymium (glass) laser [4, 7]) soon came into use.

A variety of phenomena was observed: Dielectric breakdown, plasma formation with white light generation, shock wave emission and bubble formation. As to dielectric breakdown, it was found to occur beyond a certain threshold value of laser power only, without details given at this first stage of development of the research area. Among the first quantitative results are data for plasma temperatures and shock wave strenghts. A plasma temperature of 15 000 K was measured from the flash of white light emitted during breakdown by comparing the measured spectrum with spectra of blackbody radiation [6]. Pressure waves of about 500 bar were detected at a distance of 3 mm from the breakdown site, measured with a broadband acoustic probe (a hydrophone) [3]. A sharp, audible click is reported accompanying the breakdown phenomenon. The frequency content could be measured up to 2.4 GHz with the higher frequencies being damped less than to be expected for water at the respective frequencies, indicating a shock wave, where energy from the lower frequency components is fed into the higher ones. Shock waves of 230 kbar were determined from the shock velocity in water of 7 000 m/s, when focusing the laser beam onto a submerged solid (metal) surface (platinum wire) [4]. Also photographs (shadowgraphs) of the shock waves are given there.

As to bubble formation, at first many bubbles and strings of bubbles along the optical axis of the (weakly focused) laser beam were noticed [1, 2, 3, 4]. A single bubble with its shock wave is given by Carome et al. [5], the bubble being described as “The small dark circle is the shadow of a slowly expanding region of the liquid affected by thermal diffusion and other processes occurring about the point of breakdown”. This bubble was obtained in a dust free sample of distilled water. In tap water multiple breakdown sites were observed. The complete cycle of the phenomena following laser induced breakdown including bubble expansion and collapse has first been described by Felix and Ellis [7]. They even noted several types of bubbles in their experiment with Q-switched pulses of 50 ns duration from a neodymium glass laser: A big one lasting about 650 μs, many small ones around the focal region suggested to come from the tension part of the shock wave radiated during breakdown, the bubbles lasting for about 100 - 200 μs, and many small bubbles appearing in the

"up-beam" conical focal region suggested to be formed by the temperature rise due to radiation absorption.

In the 1970s, the aspect of bubble formation by laser induced breakdown has been emphasized by Lauterborn [9, 11] and Lauterborn and Bolle [12] who investigated the dynamics of the breakdown bubble or bubbles by high speed photography and later high speed holography (Lauterborn and Ebeling [13]) as a means to further the investigation of cavitation bubble dynamics in general. Buzukov and Teslenko [8] and Akmanov et al. [10] focused their work on laser induced bubble collapse luminescence. In [9], besides high speed photography of the laser generated bubble or bubbles, the shock wave emitted upon breakdown is observed via the compression of a small bubble nearby, confirming and extending the shock wave measurements of Carome et al. [3]. In [11], among other results, the three different types of bubbles found by Felix and Ellis [7] for neodymium glass laser light are also found upon focusing pulsed ruby laser light into water and are documented by high speed cinematography (Fig. 1). The focal cone bubbles (also visible in the "down-beam" cone) form dense clouds and reappear upon collapse of the laser generated main bubble, as do the bubbles scattered in a spherical region around the breakdown site. Both bubble populations have a life time much shorter than the main bubble, because they are much smaller. They are both induced by shock waves, in their first life cycle from the shock wave of the laser induced breakdown process, and in their second life cycle from the shock wave of the bubble collapse process, as they do not appear with the unfocused laser beam. Their first appearance presumably is caused by vaporization around impurities due to absorption of the laser light and the subsequent compression with rebound leading to an enlargement of the nuclei or, else, by compression and rebound of preexisting gaseous nuclei. The second appearance can only be due to compression and rebound of preexisting nuclei as no laser beam is present. This is confirmed by the observation that many of the bubbles appearing in the first cycle also can be found in the second cycle. In [12], the dynamics of a laser generated bubble in the neighborhood of a solid boundary is investigated to study the peculiar high speed liquid jet formation towards the boundary experimentally for comparison with theory [14]. In [13], photographs of the breakdown shock waves and breakdown bubbles are given from reconstructed 3D images of holographically taken sequences. In these images the intense white light from the breakdown plasma is suppressed (see section 3). Teslenko [15] investigated the dependence of the maximum bubble radius and of the maximum pressure of the breakdown shock wave (hydrophone response time 100 ns) at a distance of 1.5 cm from the breakdown site on laser pulse energy (Q-switched ruby laser with pulse energies between 0.1 and 1 J, pulse durations between 10 and 70 ns, focal length of the focusing lens 2 cm). In distilled, degassed water he found maximum radii between about 0.25 and 0.6 mm and maximum pressure values between about 50 and 100 bar (at a distance of 1.5 cm). He also gives breakdown shock wave strength versus maximum bubble radius and finds, that more laser light energy is converted to mechanical energy for shorter laser pulses (in the range 10 ns to 70 ns). Ebeling [16] developed a theory and numerical code to describe bubble expansion and collapse with shock wave emission. The unknown initial conditions were determined

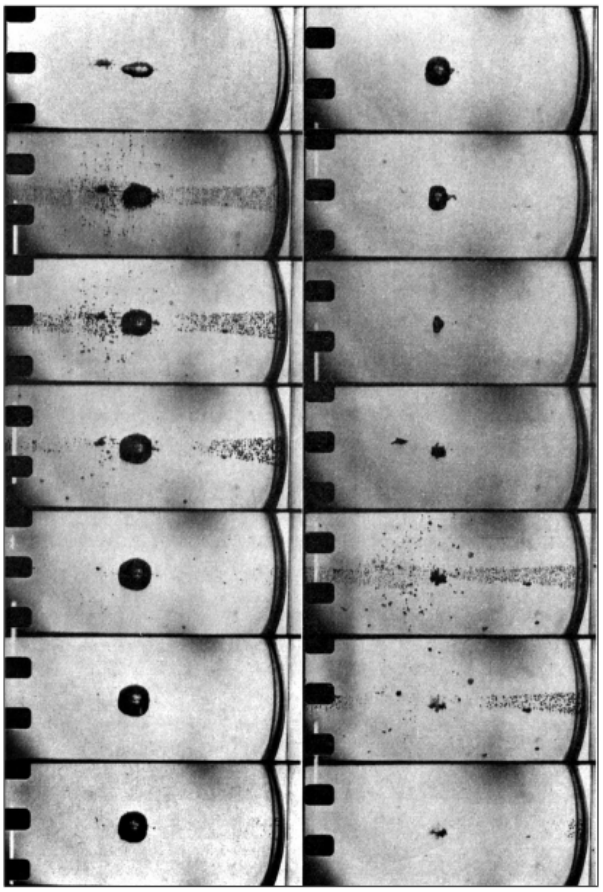

Fig. 1 Laser generated breakdown bubble in water with shock wave induced focal cone bubbles (in the upper part of the left film strip and the lower part of the right film strip) and bubbles scattered in the vicinity of the breakdown bubble site (in the upper frames of the left film strip) and bubble collapse site (in the lower part of the right film strip). Spherical flask with 250 ml at reduced pressure of 400 Torr. The time between frames is 167 μs. The Q-switched ruby laser beam (30 ns to 50 ns pulse width, wavelength 694.3 nm) is focused from the right [11].

iteratively to fit the maximum bubble radius attained and the rebound oscillations. To find good parameters for both the breakdown shock wave and the bubble collapse shock wave simultaneously proved difficult, presumably mainly due to internal processes in the bubble not being considered, for instance heat conduction and mass transfer processes (evaporation and condensation). At the end of the 1970s a collection of articles appeared covering the aspect of laser induced breakdown, called "optic cavitation", with examples of breakdown shock waves, bubble formation, collapse shock waves, jet formation (near a solid boundary and initiated by bubble

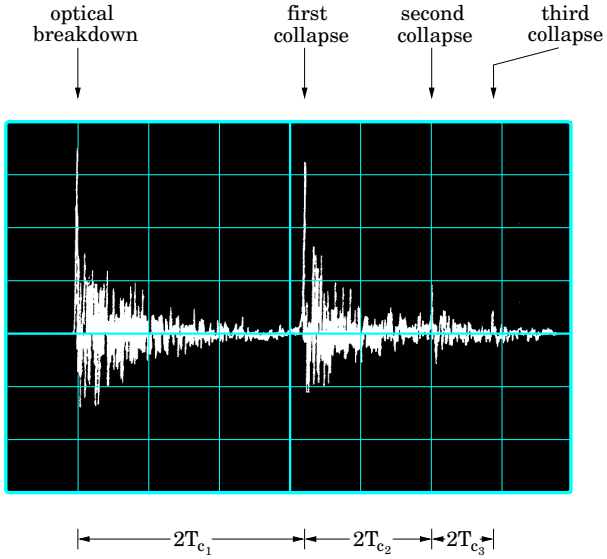

Fig. 2 Hydrophone signal from the pressure pulses emitted during laser induced breakdown and from the subsequent bubble collapses. Q-switched ruby laser pulse. T_c is the collapse time from the preceding maximum bubble radius. (Adapted from [31] in a design of Thomas Kurz).

interaction), bubble collapse luminescence and holographic generation of multiple laser induced breakdown sites [17, 18, 19, 20, 21, 22].

In the 1980s, the aspect of shock wave generation and bubble formation has been resumed by Hentschel and Lauterborn [23, 24, 25], Shima and coworkers [26, 27, 28], Fujimoto et al. [29], Vogel et al. [30, 31, 32] and Zysset et al. [33]. In these years, medical applications of shock wave generation and bubble dynamics were emerging, mainly for intraocular microsurgery [30] and lithotripsy of kidney stones [34]. The width of the shock waves (full width at half maximum of the pressure pulse) at breakdown and at bubble collapse could be determined. They were found to be about the same and lie in the range of 20 to 30 ns [31]. Also the pressure amplitudes were found to be approximately the same for the breakdown shock wave and the bubble collapse shock wave and to amount to about 60 kbar for a bubble reaching a maximum radius of $R_{\max} = 3.5$ mm. The maximum radius, $R_{\max}$, was found to scale with the cube root of the laser pulse energy over a large range of laser pulse energies for ns and ps laser pulses [33]. An example of a pressure signal from Q-switched ruby laser induced breakdown and the subsequent bubble dynamics is given in Fig. 2 in low time resolution. Four shock waves can be seen, the first one from the breakdown, the second one from the first collapse of the laser generated bubble and the two further ones from the successive collapses of the bubble. Seen from the shock waves, it seems as if the first collapse inverts the breakdown process, inasmuch as light is emitted at bubble collapse from a collapse plasma [8, 10].

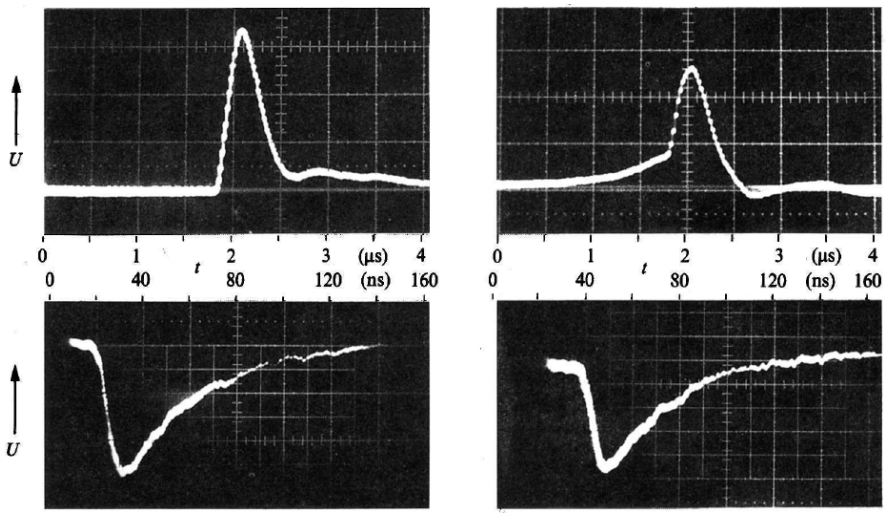

Fig. 3 Hydrophone signals of the pressure pulse (upper row) emitted at laser induced breakdown (left) and at the subsequent bubble collapse (right). Distance between hydrophone and laser induced bubble site is 8 mm. In the lower row the respective signals are shown taken with an optical detection system at a distance of 1.2 mm from the breakdown site. Q-switched ruby laser pulses of energy 200 mJ. (Adapted from [32]).

Typical pressure pulses from a PVDF hydrophone with a rise time of 145 ns and from a photodetector with a temporal resolution of 10 ns are shown in Fig. 3. The breakdown pulse features a steep rise, whereas the collapse pressure pulse is preceded by a relatively slow pressure rise within 1 to 2 μs followed by a steep rise of the shock wave detaching from the bubble. This can be explained by the pressure buildup in the liquid near the bubble during collapse as a result of the inflowing liquid that is not present in the breakdown [35, 36].

The subsequent years from the 1990s to the present have seen a wealth of investigations on laser induced breakdown in liquids with bubble and shock wave formation as applications were emerging and expanding, in particular in the medical area. These investigations are presented in the next sections and ordered in the sequence of the phenomena occurring. In section 2, the conditions for breakdown (irradiance, pulse width, pulse energy of the laser light) and the first steps of the breakdown (plasma formation, temperature and pressure buildup) will be discussed. In section 3, the focus is on the shock wave emission at breakdown (measurement, pressure distribution and propagation). In section 4, bubble formation and its dynamics is discussed and in section 5, shock wave emission at bubble collapse is presented. The chapter closes with section 6 on applications that emerged, for instance in cavitation physics, pulsed laser ablation, laser lithotripsy and micro- and nanosurgery.

2 Laser Induced Breakdown in Liquids

Laser induced breakdown and plasma formation in pure, transparent liquids (water) is effected by a combination of photoionization, inverse Bremsstrahlung absorption, and cascade (avalanche) ionization to yield free electrons that in larger amounts, together with the positive ions, form a plasma [37, 38, 39]. The processes taking place during breakdown are depicted in Fig. 4. Here, water is modeled as an amorphous semiconductor [40] as "the breakdown probability has a dependence on the laser field similar to that found in solids" [41].

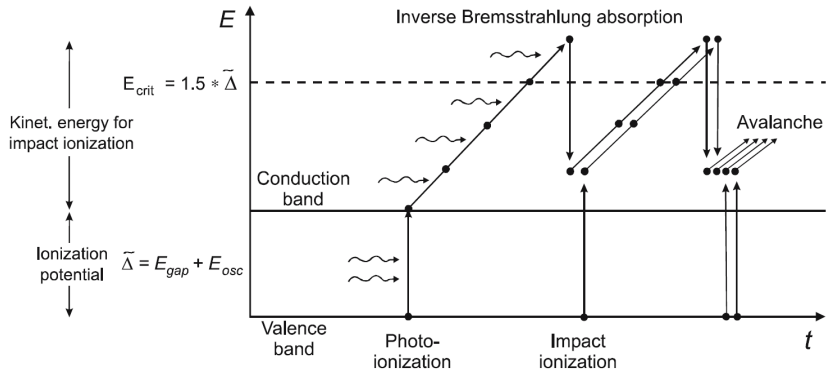

Fig. 4 Visualization of photoionization, inverse Bremsstrahlung absorption and impact ionization leading to photoinduced breakdown and plasma formation. (After Vogel et al. [39]).

Avalanche breakdown only starts, when quasi-free seed electrons are present in the conduction band that are usually produced by photoionization of the liquid molecules through multiphoton absorption or tunneling. Impurities in the liquid may significantly lower the breakdown threshold through the easier production of seed electrons by absorption. The seed electrons then may absorb laser photons by inverse Bremsstrahlung absorption, thus gaining kinetic energy. Once the kinetic energy sufficiently exceeds the effective ionization potential, the electron may transfer part of its energy to a bound electron by a collision (or impact) to generate a further seed electron (impact ionization). The two seed electrons repeat the uptake of energy from the laser beam by inverse Bremsstrahlung absorption and impact ionization starting a cascade with exponential increase of electrons. Loss mechanisms (inelastic collisions, diffusion of electrons out of the laser beam) lead to a threshold in irradiance for breakdown to occur and a plasma to be formed [38]. The energy of the free electron is transferred to the molecules by collisions and electron-hole recombinations, which leads to a rapid rise of temperature and pressure.

A table of measured thresholds has been compiled by Vogel et al. [39], whereby different definitions for the breakdown threshold are considered (visible plasma light emission; detectable bubble). Threshold values are in the order of 10^{11} W/cm^2 for pulses with a few ns duration and 10^{13} W/cm^2 for 100-fs pulses. Data exhibit large

variations of the order of one magnitude, due to the statistical nature of the breakdown (for ns pulses) and varying experimental conditions in different experiments.

Whereas the breakdown threshold is difficult to determine, the extent of the plasma formed can easily be measured by photographic means [42, 43, 44]. Figure 5 gives the plasma length in the direction of the laser beam for 6 ns and 30 ps Nd:YAG laser pulses in dependence on laser pulse energy (a) and on the normalized laser pulse energy (b), normalized with the threshold energy E_{th} (2.4 μJ for 30 ps pulses, 141 μJ for 6 ns pulses). The plasma length is considerably larger for ps laser pulses ($\sim$2.5 times larger in this typical case of pulse widths and at the same pulse energy). However, when the same data are plotted versus the normalized laser pulse energy, the ns pulses show a larger plasma length. This is due to the larger volumetric energy density achieved at longer pulse durations that results in plasma enlargement due to radiative energy transfer [43].

The maximum temperature in the breakdown plasma is found spectroscopically to lie between 6000 K and about 15 000 K for ps and ns laser pulses [37]. Subpicosecond laser pulses may lead to optical breakdown with detectable bubble

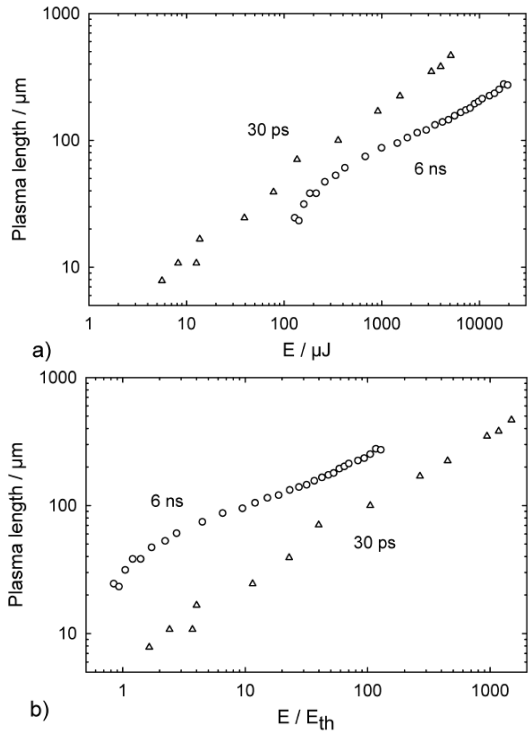

Fig. 5 Plasma length as a function of laser pulse energy (a) and normalized laser pulse energy (b) for ns and ps pulses focused into distilled water. Nd:YAG laser, wavelength 1064 nm, 30 ps and 6 ns pulses. Focusing angle 22°. (After Vogel et al. [43]).

formation but without detectable light emission. Therefore, temperature values connected with the breakdown can not yet be given for all cases.

Besides the temperatures, the pressures in the breakdown plasma are of interest. The pressure buildup in the breakdown volume can not be measured directly, but may be inferred from the temperature rise or the initial velocity of the shock wave at the rim of the plasma. The thermalization of the kinetic energy carried by the free electrons heats the focal volume without time being left for acoustic relaxation for short laser pulses. Therefore, at the end of the laser pulse (ps or fs duration), the maximum pressure is attained [39]. The pressure developed during plasma formation will act as a disturbance in the liquid and propagate away from the breakdown volume into the liquid. There, it can be measured with a fast hydrophone or by optical means [29, 31, 32, 45, 46] as a pressure pulse or shock wave. These investigations are discussed in the next section on shock wave emission (section 3).

A more thorough account of the conditions for and processes at laser induced breakdown (LIB) can be found in Kennedy et al. [37], mainly for ns and ps laser pulses, in Noack and Vogel [38], and in Vogel et al. [39], mainly for fs pulses. In these reviews, multiphoton, impact and avalanche (cascade) ionization are discussed in depth. Kudryashov and Zvorykin [47], starting from their experiments with ($248\,\mathrm{nm}, 25\,\mathrm{ns}, <0.12\,\mathrm{J}$) KrF laser pulses, discuss a new pathway to electron avalanche evolution by considering the influence of the dissociation of water molecules to free radicals (mainly H and OH) on the breakdown sequence of events.

A different model for laser induced breakdown has been proposed by Byun and Kwak [48] for the case of not extremely high laser power and pulses of duration above the order of picoseconds. They treat laser induced plasma formation as a phenomenon of laser induced thermal breakdown resulting from an absorption driven temperature rise to the superheat limit with subsequent explosive evaporation starting at the center of a spherical volume defined by the focal volume of the focused laser beam where the pulse energy is deposited. That way they arrive at initial conditions from where to start calculations of shock wave emission and (vapor) bubble growth. The authors report a reasonable agreement with experimental data of shock wave strength from Noack et al. [49].

3 Shock Wave Emission at Breakdown

When investigating laser induced breakdown, it was soon noticed that shock waves were produced, visible in photographs or shadowgraphs of the breakdown area [4]. The exposure time of the photographs must be short enough to stop the motion of the shock wave. Today this presents no problem with short laser pulses and short electronic shutter times. However, the bright light emitted during breakdown may overexpose the optical sensor or photographic material blurring the breakdown site. A method to overcome this experimental difficulty is high speed holography, where a scene is illuminated by coherent light and the image stored in the hologram is reconstructed with the same coherent light [13]. Then the incoherent light from the

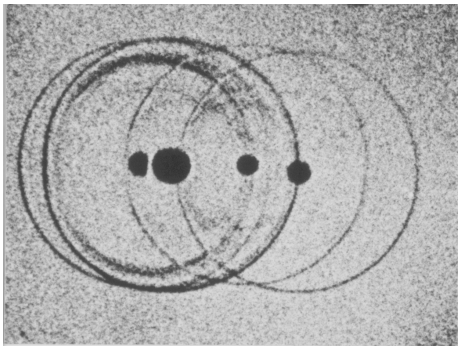

Fig. 6 Shock wave emission and bubble formation after Q-switched ruby laser induced breakdown in water. Reconstructed image of a hologram taken 1.75 μs after breakdown. Laser beam coming from the right. Picture size is (height $\times$ width) 1.1 mm $\times$ 1.6 mm [13].

plasma is not recorded as an image, but only constitutes a continuous background on the hologram that is not reconstructed. An example of a breakdown process taken holographically is given in Fig. 6. Bubbles and shock waves, even the reflections of shock waves at neighboring bubbles, can be seen that otherwise would have been lost. The threedimensional structure of the shock waves is also present when looking through the hologram, but difficult to transfer to normal print. The method has even been extended to high speed holocinematography [20, 50, 24, 25]. The trend for digital photography has not yet lead to an equivalent digital holography and thus this experimental tool is at present outdated. Holography, however, has seen a renaissance in producing laser induced breakdown with intended multiple breakdown sites. Whereas in the first attempts [18, 22] the holographic material had to be properly exposed and chemically processed to arrive at a phase only hologram, modern digital spatial light modulators may directly serve as a phase hologram for producing multiple breakdown sites, for instance for bubble interaction studies [51], nonspherical bubble generation [52] and multi-point laser microsurgery [53].

By using large image magnification together with bright illumination, overexposure by the plasma irradiation can be avoided, and photography, shadowgraphy or schlieren photography are sufficient to follow the shock waves and bubble growth in time. Figure 7 gives an example for a (10 mJ, 6 ns) laser induced breakdown event [45]. Each frame is a photograph from a different laser shot, but due to the excellent reproducibility of the event sufficiently far beyond the breakdown threshold a sequence can be constructed giving the evolution of plasma formation, shock wave emission and bubble formation and expansion. The detachment of the shock front from the plasma occurs immediately after plasma formation, because its velocity is always larger than the particle velocity behind the shock front. This can be seen in the first frame of Fig. 7. The plasma formation begins at the beam waist and grows into the incoming focal cone of the laser beam as long as the laser beam lasts [54]. The shock wave first detaches from the plasma tip whereas the plasma tail is

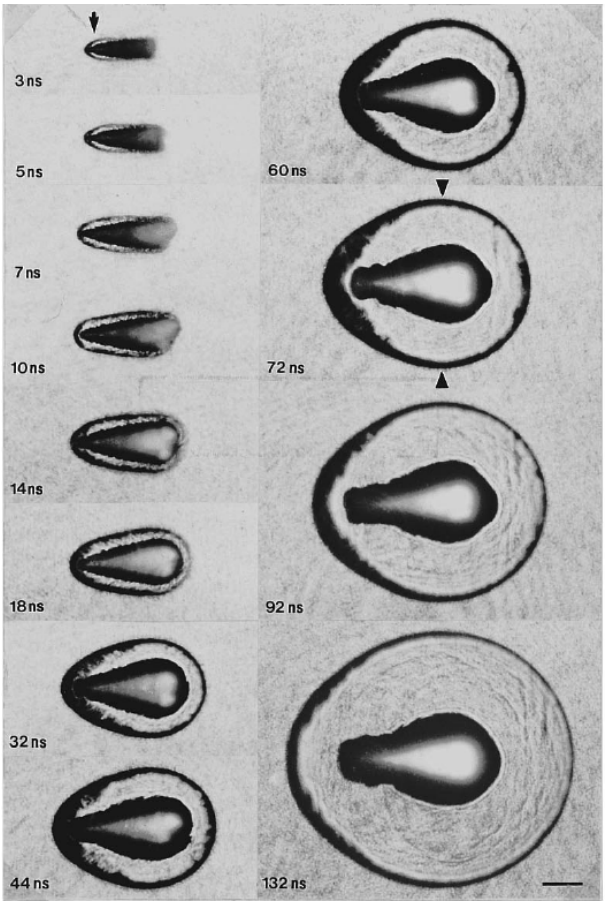

Fig. 7 Shock wave emission and bubble formation during the initial phase of laser induced breakdown in water. The Nd:YAG laser beam of wavelength 1064 nm is focused from the right. Laser pulse of 6 ns duration and 10 mJ energy. Scale bar = 100 μm. The focal point is given by the arrow in the first frame (upper left). The arrowheads in the second frame of the second row show the section through the photographs, where the shock wave radius and the bubble radius have been measured. (After Vogel et al. [45]).

still growing fed by the laser pulse. More details on plasma formation, shock wave emission and the initial phase of bubble formation can be found in [43, 45].

From these and similar pictures the propagation of the shock front and bubble wall motion have been determined by direct evaluation. In Fig. 8, the distance of the shock front and of the bubble wall from the optical axis is given in dependence on time for the (10 mJ, 6 ns) laser pulse (see Fig. 7). Similar diagrams are obtained for picosecond [45] and femtosecond [55] breakdown. It is noticed that the velocity of the shock wave slows down with time as does the bubble wall velocity. The

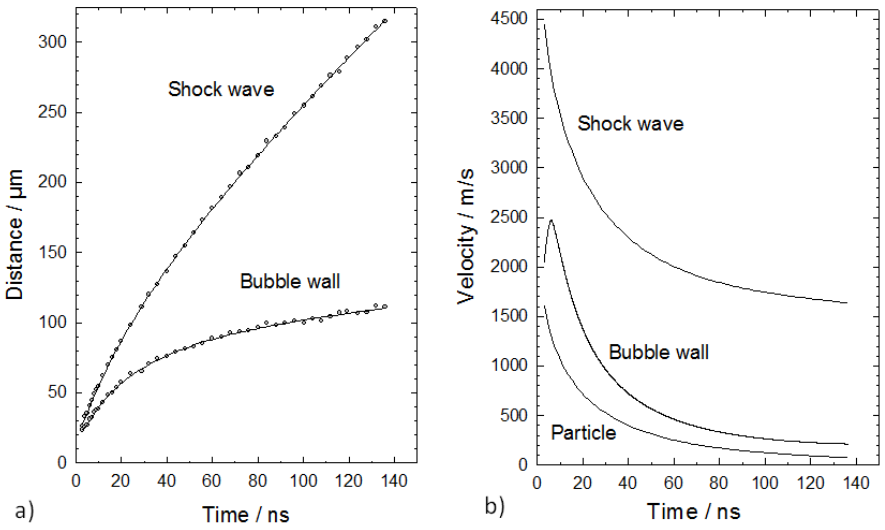

Fig. 8 Shock wave propagation and bubble wall expansion (left) and velocity (right) perpendicular to the optical axis after laser induced breakdown in water. The time axis gives the delay between laser pulse and illumination pulse. Nd:YAG laser pulse at 1064 nm wavelength, 10 mJ pulse energy, 6 ns pulse duration, focal cone angle in water 22°. (After Vogel et al. [45]).

initial (maximum) shock front velocity is as high as 4450 m/s (three times the normal sound speed in water). Also the initial (maximum) bubble wall velocity is supersonic (2450 m/s). In the case of femtosecond laser induced breakdown in water 10 times above the energy breakdown threshold (100 fs, 800 nm, 1 μJ), a very fast plasma extension has been observed by means of a light scattering technique with the shock wave detaching after about 800 ps with an initial velocity of 5200 m/s [56]. The slowing down of the shock wave seen in Fig. 8 is partly due to the geometrical factor of spherical expansion and partly caused by energy dissipation at the shock front [45, 57], both effects decreasing the peak shock pressure and thereby the propagation velocity. The slowing down of the bubble wall is mainly due to the transfer of the plasma energy into potential energy of the bubble by the work of the expanding bubble done against the outer static pressure.

The measurement of shock wave pressures at laser induced breakdown is not an easy task, but has been refined over the times. Conventional hydrophones suffer from their large time constant (the fastest have time constants larger than 10 ns) and relatively large sizes. Optical methods, where the shock wave propagation is imaged [45, 46], the shock wave passes the focus of a laser beam [29, 31] or is reflected at the tip of a fiber [58], reach ns resolution. For the shock wave pressures it is found that they are generally higher for ns laser pulses than for ps laser pulses (same energy per pulse). The reason is that the breakdown threshold is lower for picosecond pulses and therefore the energy is deposited in a larger volume than for

ns laser pulses leading to a higher energy density, temperature increase and thus pressure for ns laser pulses. Pressure conditions can now be determined even down to 4 μJ laser pulse energy [59]. Thereby it has been found for ns laser pulses that there is only a weak dependence of the shock wave strength on laser pulse energy. When going from 8 μJ to 10 mJ laser pulse energy, there is only an increase from 20 kbar to about 70 kbar peak pressure. The increase of shock wave energy with laser pulse energy is largely reflected in a broader shock wave width. The efficiency of the transformation of laser light energy into mechanical energy (shock wave energy and bubble energy (see below)) becomes lower for decreasing numerical aperture [57].

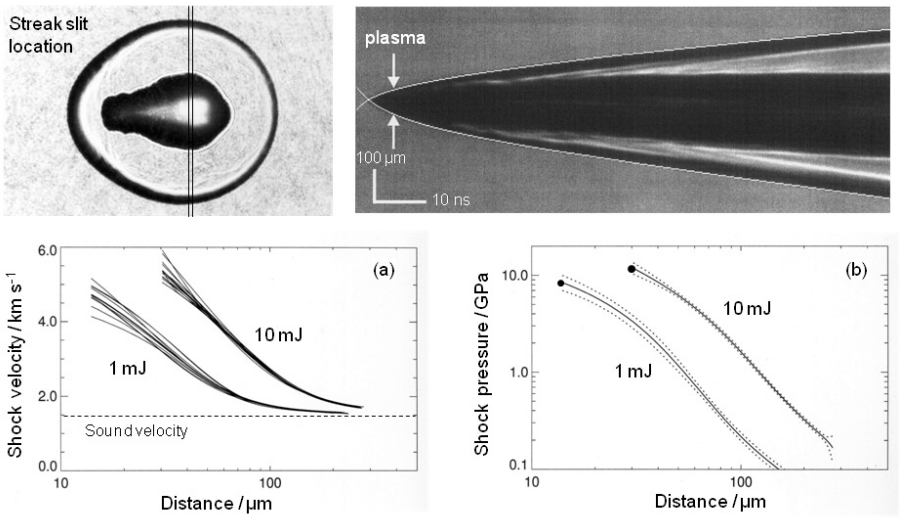

Fig. 9 Determination of shock wave strength from streak recordings. Upper left: The slice through the object image. Upper right: A streak image for a (5 mJ, 6 ns) Nd:YAG laser pulse focused into water with a focusing angle of 22°. Lower left: Dependence of shock wave velocity on distance traveled. The bunches are from separate measurements (shock waves). Lower right: Dependence of shock wave peak pressure on distance traveled. The dotted lines give the standard deviation, the thick dots denote the plasma rim. (After Noack and Vogel [46]).

The maximum shock wave pressure during laser induced breakdown, i. e. the pressure at the plasma rim, and the subsequent propagation of the shock wave can best be visualized and obtained by streak photography [49, 46]. The position $r(t)$ of the shock front is extracted from the streak image (see Fig. 9, upper right image) as a function of time (compare Fig. 8), whereby image processing techniques may be used [46]. Differentiation of the $r(t)$ curve with respect to time yields the shock wave velocity u_s. It is related to the shock peak pressure p_s, according to [45], by

$$p_s = c_1 \rho_0 u_s (10^{(u_s - c_0)/c_2} - 1) + p_{stat}\,, \tag{1}$$

where $c_0 = 1483$ m/s is the sound speed and $\rho_0 = 998\,\mathrm{kg/m^3}$ the density of the undisturbed water. $c_1 = 5190$ m/s and $c_2 = 25\,306$ m/s are empirical constants determined from Rankine-Hugoniot data for water by Rice and Walsh [60], and p_{stat} is the static pressure in the liquid.

In Fig. 9, the procedure for determining the shock wave pressure evolution during propagation from the source (optical breakdown site) via a single streak recording is depicted. First, a slit must be positioned appropriately to obtain an image slice of the object at the expected source of the shock wave for complete coverage of the shock wave pressure evolution (see Fig. 9, upper left image). The streak image then records the propagation of the shock wave in a distance-time diagram, the distance being recorded along the vertical axis, the time along the horizontal axis (see Fig. 9, upper right image). The outer boundary, here marked by a white curve obtained by picture processing, is the shock front. A high resolution of 6.4 μm in space and 200 ps in time has been achieved (see [46]). From the white curve, the velocity $u_s(r,t)$ can be obtained by differentiation with respect to time for each location r of the shock front (see Fig. 9, lower left diagram). From $u_s(r)$ with eq. (1) the shock wave pressure curves $p_s(r)$ are determined (see Fig. 9, lower right diagram). Data are shown for a 6 ns Nd:YAG laser pulse in water for the two pulse energies of 1 mJ and 10 mJ; the streak example in Fig. 9 is for a pulse energy of 5 mJ. The maximum shock wave velocities measured are 4700 m/s (1 mJ) and 5400 m/s (10 mJ), the corresponding shock wave velocities calculated amount to 84 kbar and 118 kbar, respectively.

Peak shock wave pressures of 30 to 90 kbar are obtained at sixfold energy breakdown threshold in a survey of ns, ps, and fs breakdown [49]. An exception of only 3 kbar has been found for the 3 ps laser pulse. This can be understood by the finding that the absorption coefficient of the laser induced plasma is lowest around about 3 ps [38, 57]. The (100 fs, 800 nm, 1 μJ) laser pulse of [56] leads to 110 kbar peak shock wave pressure, but at tenfold energy breakdown threshold. Vogel et al. [39],

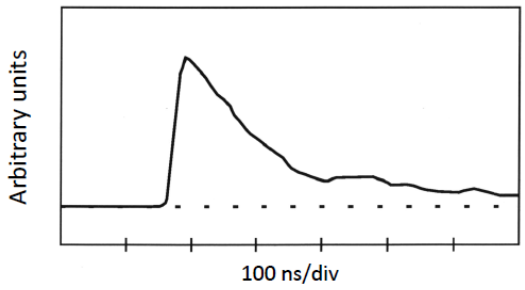

Fig. 10 Hydrophone signal of the shock wave emitted at laser induced breakdown for a bubble reaching a maximum radius of 700 μm. The rise time of the hydrophone is 12 ns, the distance to the laser induced bubble site 3 mm. The full width at half maximum of the shock wave is 70 ns. (Measurement by A. Vogel).

on the other hand, determined a peak pressure of 10 kbar at thirtyfold threshold energy for a 100 fs laser pulse.

The pulse duration of the shock wave or its precise form can only roughly be estimated from its width on photographic or streak images (together with the propagation speed of the shock wave) due to the complicated image forming process involving the camera settings. However, this is possible with optical deflection measurements [31] and with sufficiently fast hydrophones. With a hydrophone of rise time 12 ns, the shock width has been determined to 120 ns for the 76 ns laser pulse and to 80 ns for the 6 ns laser pulse at a distance of 10 mm and 9 mm from the breakdown site, respectively [49]. An example for the form of the shock wave as measured with a fast hydrophone is given in Fig. 10. The distance of the PVDF hydrophone from the breakdown site is 3 mm. A steep rise is followed by a relatively slow decay. It is a monopolar pulse, because the plasma in water acts as a free surface and is not able to sustain a tension. However, in elastic-plastic tissue-like media the stress transient is bipolar with the tensile part reaching an amplitude of up to 40% of the compressive stress [61]. Furthermore, pressure transients are bipolar under stress confinement conditions. Here, the tensile part of the stress wave will support bubble formation for energies close to the threshold [39].

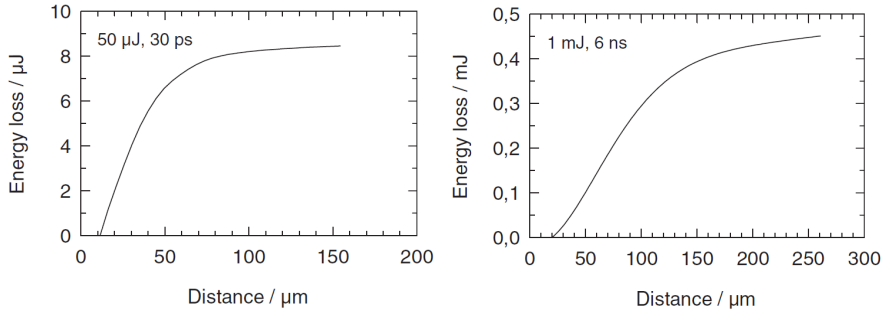

Fig. 11 Experimentally determined shock wave decay (accumulated energy loss) with distance travelled for a 30 ps (left diagram) and a 6 ns laser pulse (right diagram). (After Vogel et al. [57]).

The dissipation of the shock wave is available via the measurement of the shock front velocity u_s, when measured as a function of r, the propagation distance. The procedure for determining the energy loss from $u_s(r)$ is described by Vogel et al. [57]. Figure 11 gives the results for two laser pulse parameters. The energy loss is high immediately after detachment from the plasma and gets almost negligible as soon as the propagation velocity reaches the linear sound speed in the liquid. As most of the acoustic energy is dissipated in the first few 100 μm, a farfield measurement of the acoustic energy radiated at laser induced breakdown strongly underestimates the energy carried away by the shock wave.

4 Bubble Formation and Subsequent Dynamics

When the shock wave has detached from the plasma, there is still left a volume of high pressure and temperature not in equilibrium with the surroundings. This volume expands more slowly than the shock wave doing work against the outer pressure. In most cases, the outer pressure is the ambient static pressure, p_{stat}, and the potential energy, E_{pot}, gained by this work is, according to standard formulae, when V is the final volume, $E_{\mathrm{pot}} = \int p_{\mathrm{stat}} \mathrm{d}V = p_{\mathrm{stat}} V$. In the present case of water, disregarding chemical reactions inside the plasma (for instance dissociation of the water molecules by the high temperature and recombination upon cooling during expansion), the expanding volume will soon be filled with water vapor of pressure p_{v}. If the final volume, when the energy of the plasma is used up, is a spherical bubble of maximum radius R_{max}, as often seen in experiments, the energy stored in the bubble, E_{B}, is given by

$$E_{\mathrm{B}} = \frac{4\pi}{3}(p_{\mathrm{stat}} - p_{\mathrm{v}})R_{\mathrm{max}}^3. \tag{2}$$

After the bubble has reached the maximum radius, the interior pressure is p_{v} (2.33 kPa in water at 20 °C), much smaller than the outer pressure p_{stat} (normally about 1 bar = 100 kPa), and the bubble will be compressed back to a small volume, inverting the expansion. Upon collapse of the bubble, in the final stage a light flash is emitted [8, 10, 62], a shock wave is launched into the liquid, similarly to that one at bubble expansion and the bubble rebounds (expands again) to a smaller maximum radius, as energy is lost, mainly to the collapse shock wave. An example of bubble expansion, collapse and rebound following an 8 ns Nd:YAG laser pulse in water is given in Fig. 12 [63]. The bubble reaches a maximum radius of about 750 μm. It is observed that the rebound bubble is no longer spherical. The reason is that bubble collapse is an unstable process that suffers from the Strube instability [64].

Equations for the dynamics of spherical bubbles have been formulated in several degrees of approximation. The simplest one is the Rayleigh model [65]:

$$\rho R\ddot{R} + \frac{3}{2}\rho\dot{R}^2 = p_{\mathrm{i}} - p_{\mathrm{e}}\,. \tag{3}$$

Here, R is the bubble radius, an overdot means differentiation with respect to time, ρ is the density of the liquid. The difference in pressure, $p_{\mathrm{i}} - p_{\mathrm{e}}$, drives the bubble motion, where p_{i} is the pressure inside the bubble and p_{e} is the external pressure in the liquid. The form of the inertial terms on the left-hand side is due to the spherical three-dimensional geometry that is transformed to one radial dimension in the differential equation.

This equation can be integrated to calculate the time from the bubble maximum to the subsequent minimum to get the Rayleigh collapse time, when $p_{\mathrm{i}} - p_{\mathrm{e}}$ is constant ($p_{\mathrm{i}} = p_{\mathrm{v}}$ = the vapor presssure in the bubble, $p_{\mathrm{e}} = p_{\mathrm{stat}}$ = the static ambient pressure):

$$T_{\mathrm{c}} = 0.915\, R_{\mathrm{max}} \sqrt{\frac{\rho}{p_{\mathrm{stat}} - p_{\mathrm{v}}}}. \tag{4}$$

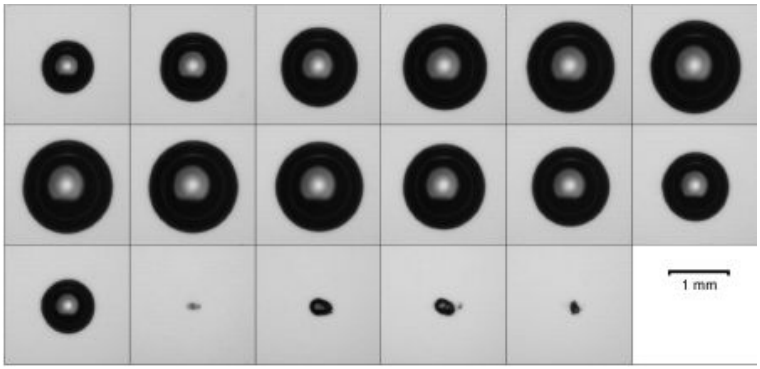

Fig. 12 Photographic series of spherical bubble expansion, collapse and rebound of a laser generated bubble in water. The series starts 10 μs after breakdown. Interframe time 10 μs, 8 ns Nd:YAG laser pulse. Maximum bubble radius about 750 μm. Backlight conditions through a diffusive screen. (After Kröninger et al. [63]).

This relation has been confirmed experimentally for laser bubbles in water (e. g. [11]) and can be used inversely to determine R_{max} from measured T_c [23]. For small bubbles (less than 1 μm) surface tension will influence the relation between R_{max} and T_c and must be taken into account [66, 67]. Whereas R_{max} needs high speed photography for direct measurement, T_c can be measured, without knowing the time instant when R_{max} is reached, just with a fast hydrophone in the following way. The time interval, T_B, from the formation of the bubble (time of laser induced breakdown) to the first collapse is $T_B = 2T_c$, when there is little damping in between, as it happens to be true for water in the cases considered. Both time instants are marked by the emission of a shock wave that can be measured with a hydrophone. As both shock waves may need different times to arrive at the hydrophone due to different propagation velocities at different strength (see eq. 1), there may occur an error in the measured instances to be corrected for ultraprecise measurements. Another way for getting T_B is by evaluating the light scattering of a cw probe laser beam (see, e. g. [68, 67]). An evaluation of T_c or R_{max} with laser pulse energy, E_L, reveals a proportionality of the maximum volume V_{max} of the bubble with E_L. Stated in terms of the potential energy, E_B, stored in the bubble at maximum radius (eq. 2): $E_B \propto E_L$. Figure 13 confirms this relation for ns and ps laser pulses that are well above the breakdown threshold for bubble formation by the slopes of the curves. A complete calculation of E_B from the measurement of T_c leads to the diagrams of Fig. 14. From the slopes of the curves the percentage of the energy of the laser pulse going into bubble energy is 19 % for the 30 ps pulses (Fig. 14, upper diagram) and 25 % for the 6 ns pulses (Fig. 14, lower diagram). The energy contained in the shock wave emitted during optical breakdown usually is about twice as large as the bubble energy [57].

A bubble model that incorporates sound radiation into the liquid from the expanding and collapsing bubble is the Gilmore model [69]. For strong collapse, i. e. strong compression of the contents inside the bubble, a van der Waals hard core law

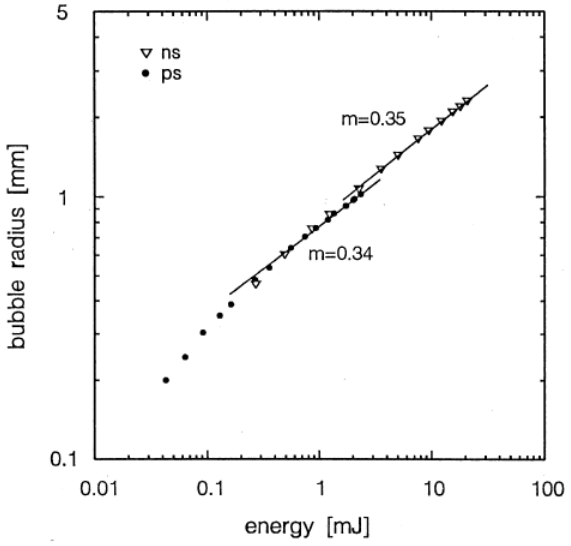

Fig. 13 Maximum bubble radius versus laser pulse energy for ns and ps laser pulses focused into water. The maximum bubble volume is proportional to the laser pulse energy when well above the breakdown threshold as seen by the slopes to the curves that are about 1/3. (After Vogel et al. [42]).

has been included to account for a noncompressible volume of the inert gas inside the bubble [70]. This bubble model reads (see also [71, 45, 72, 73]):

$$\left(1-\frac{\dot{R}}{C}\right)R\ddot{R}+\frac{3}{2}\left(1-\frac{\dot{R}}{3C}\right)\dot{R}^2=\left(1+\frac{\dot{R}}{C}\right)H+\frac{\dot{R}}{C}\left(1-\frac{\dot{R}}{C}\right)R\frac{\mathrm{d}H}{\mathrm{d}R}, \tag{5}$$

where

$$H=\int_{p|_{r\to\infty}}^{p|_{r=R}}\frac{\mathrm{d}p(\rho)}{\rho}, \tag{6}$$

$$p(\rho)=A\left(\frac{\rho}{\rho_0}\right)^{n_\mathrm{T}}-B, \tag{7}$$

$$p|_{r=R}=\left(p_\mathrm{stat}+\frac{2\sigma}{R_\mathrm{n}}\right)\left(\frac{R_\mathrm{n}^3-bR_\mathrm{n}^3}{R^3-bR_\mathrm{n}^3}\right)^{\kappa}-\frac{2\sigma}{R}-\frac{4\mu}{R}\dot{R}, \tag{8}$$

$$p|_{r\to\infty}=p_\mathrm{stat}+p(t), \tag{9}$$

$$C=\sqrt{{c_0}^2+(n_\mathrm{T}-1)H}. \tag{10}$$

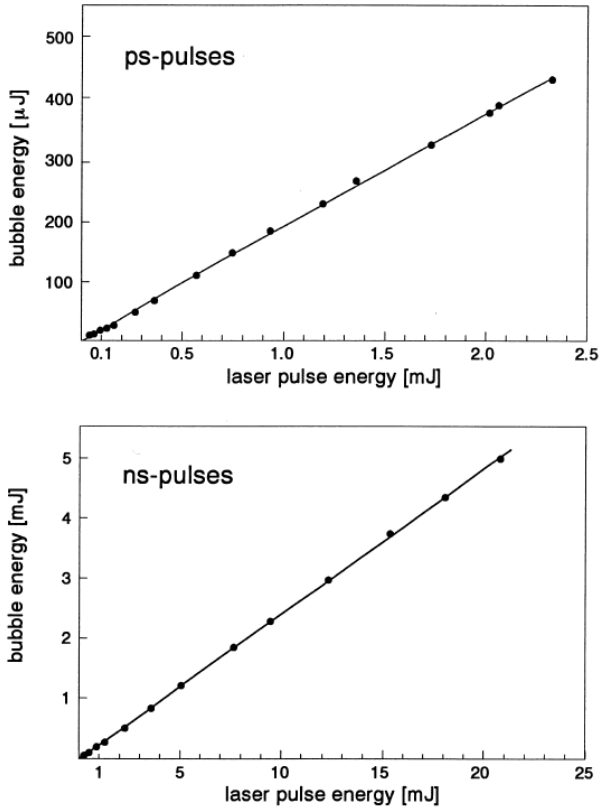

Fig. 14 Maximum bubble energy versus laser pulse energy for ps (top) and ns (bottom) laser pulses focused into water. (After Vogel et al. [42]).

The additional parameters and variables in this model are the polytropic exponent of the gas in the bubble, κ, the (dynamic) viscosity, μ, and the surface tension of the liquid, σ, the sound velocity in the liquid at normal conditions, c_0, the sound velocity at the wall of the bubble, C, the enthalpy, H, the parameters of the equation of state, where the Tait equation (7) is chosen with its parameters A, B, n_{T}, and the van der Waals constant, b. The Gilmore model was used in [39, 45] to calculate shock wave emission and bubble expansion for ns, ps, and fs optical breakdown.

A further model is the Keller-Miksis model [74] that also incorporates sound radiation from the oscillating bubble, but features a retarded time $t + R/c$ in the equations. A model equivalent to this model to first order in $1/c$, c being the sound velocity in the liquid, and dispensing with the retarded time [75, 76] reads

$$\left(1-\frac{\dot{R}}{c}\right)R\ddot{R}+\tfrac{3}{2}\dot{R}^2\left(1-\frac{\dot{R}}{3c}\right)=\left(1+\frac{\dot{R}}{c}\right)\frac{p_{\mathrm{l}}}{\rho}+\frac{R}{\rho c}\frac{\mathrm{d}p_{\mathrm{l}}}{\mathrm{d}t}, \tag{11}$$

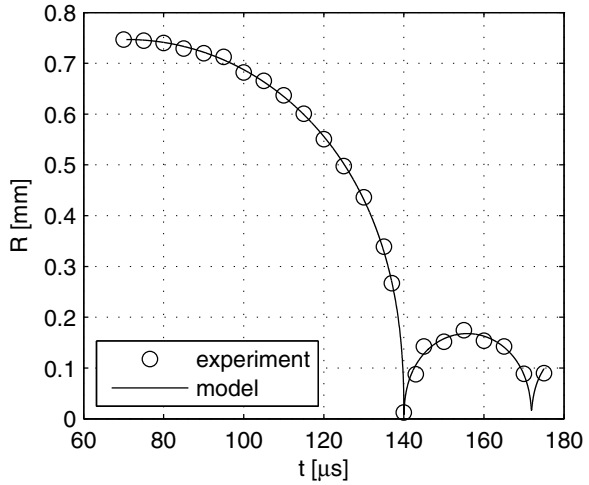

Fig. 15 Comparison of the motion of a spherical laser generated bubble in water with theory (Keller-Miksis model, eq. 11). Experimental data according to the bubble of Fig. 12. (After Kröninger et al. [63]).

with

$$p_{\mathrm{l}} = \left(p_{\mathrm{stat}} + \frac{2\sigma}{R_{\mathrm{n}}}\right)\left(\frac{R_{\mathrm{n}}^3 - bR_{\mathrm{n}}^3}{R^3 - bR_{\mathrm{n}}^3}\right)^{\kappa} - p_{\mathrm{stat}} - \frac{2\sigma}{R} - \frac{4\mu}{R}\dot{R} - p(t), \qquad (12)$$

The connection between the different bubble models has been explored by Prosperetti and Lezzi [77, 78]. Typical values of the parameters for gas bubbles in water, as used in the calculations with the Keller-Miksis model, are $p_{\mathrm{stat}} = 100$ kPa, $p_{\mathrm{v}} = 2.33$ kPa, $\sigma = 0.0725$ N/m, $\kappa = 1.67$ (noble gas) or $\kappa = 1.4$ (air), $\mu = 0.001$ Pa s, c = 1483 m/s, $\rho = 998$ kg/m^3. The pressure $p(t)$ is a time varying pressure, for instance a sound field or a pressure pulse.

The experimental bubble dynamics as given in Fig. 12 has been fitted with the Keller-Miksis model (eq. 11) to yield the comparison done in Fig. 15. It is seen that the complete dynamics can be fitted including the energy loss by the shock waves emitted upon collapse. Fit parameters are the Rayleigh collapse time $T_{\mathrm{c}} = 71\,\mu$s, maximum bubble radius $R_{\mathrm{max}} = 747\,\mu$m, and a bubble radius at rest of $R_{\mathrm{n}} = 69\,\mu$m that is needed for eq. 12.

5 Shock Wave Emission at Bubble Collapse

The collapse of a laser induced breakdown bubble is a very fast process that can be resolved photographically only by extremely high framing rates. So far, shock wave emission at bubble collapse in the bulk of water has been recorded photographically with up to 100 million frames per second [79, 80]. Figure 16 shows an example, where the shock wave emitted at laser bubble collapse has been photographed at

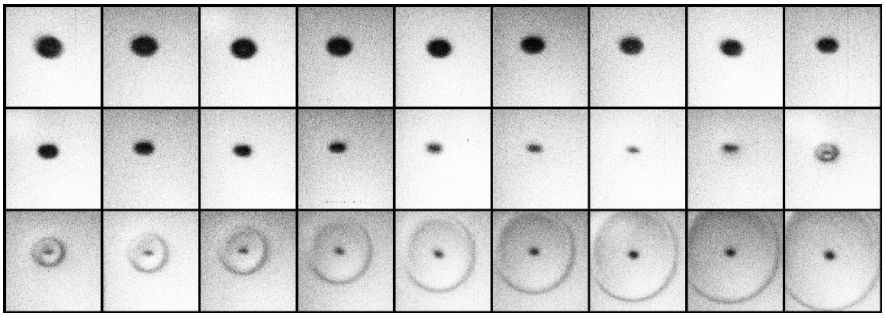

Fig. 16 Shock wave emission at the collapse of a laser induced bubble in water. Photographic series combined from several series taken at 20.8 million frames per second (interframe time 48 ns). The maximum bubble radius is 1.1 mm reached 99.5 μs before the first frame. Frame size is (height $\times$ width) 1.8 mm $\times$ 1.5 mm. (Courtesy of C. D. Ohl).

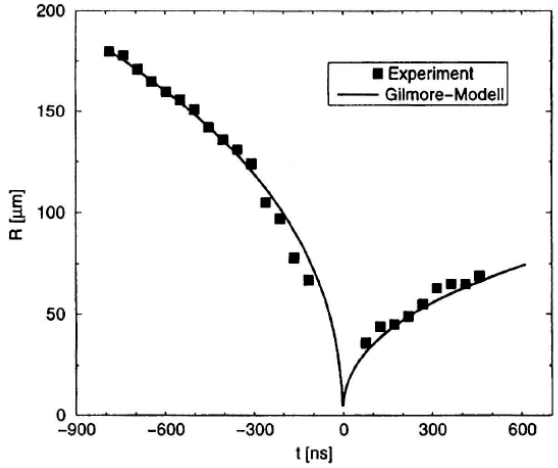

Fig. 17 Bubble wall motion at collapse of a laser induced bubble in water. Comparison of experiment (full squares, taken from the images in Fig. 16) with theory (eq. 5; solid line). Initial conditions chosen: $R(t_0) = 180\,\mu$m, $\dot{R}(t_0) = -96.2$ m/s with $t_0 = -788$ ns. The maximum radius is $R_{\max} = 1.1$ mm. The missing of the experimental points near collapse is due to the shock wave emitted at collapse that obscures the bubble inside the shock wave. (Courtesy of O. Lindau).

20.8 million frames per second by concatenation of sequences of eight frames from different breakdown events with properly shifted delay. The bubble reached a maximum radius of 1.1 mm, but only the collapse phase is shown. The bubble collapses slightly elongated as often seen with larger bubbles that are generated with slightly elongated laser plasmas.

The bubble dynamics is compared with the theory of Gilmore (eq. 5) in Fig. 17. No experimental radius values can be obtained near the collapse as the shock wave

hides the view onto the bubble surface. As the rebound radii can be fitted, the theoretical model seems adequate for the description of bubble collapse including shock wave emission. However, Fuster et al. [81] recently formulated and solved a rigorous solution for strong collapse of a bubble in a sound field and compared it (among others) with the Gilmore and Keller-Miksis approximations. For collapse pressures (in the bubble) above 1 kbar, they find up to 100 % larger pressures than in the approximations.

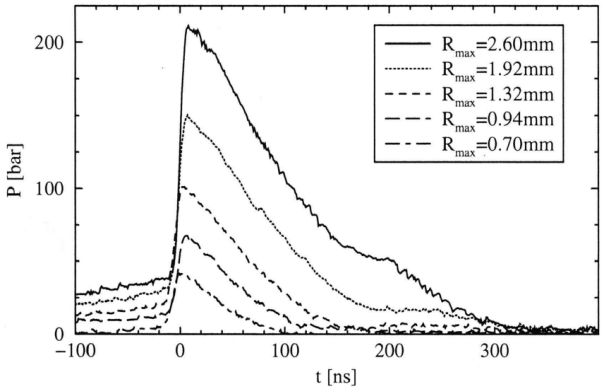

Fig. 18 Collapse of a laser induced bubble in water. Form of the first collapse pressure pulse for different maximum bubble radii attained after laser induced breakdown. Q-switched Nd:YAG laser pulse of width 8 ns. Distance of the fiber optic hydrophone from the breakdown site is $d = 3$ mm. Each curve is the average over 50 signals. (Courtesy of O. Lindau).

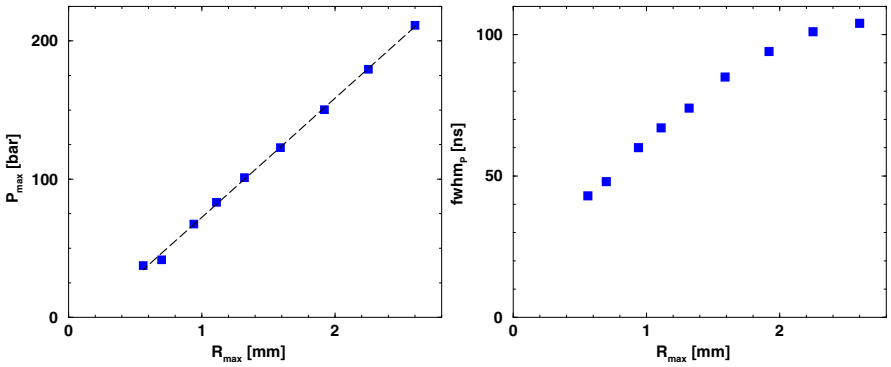

Fig. 19 Collapse of a laser induced bubble in water. Amplitude (left) and width (right) of the first collapse pressure pulse in dependence on the maximum bubble radius attained after laser induced breakdown. Q-switched Nd:YAG laser pulse of width 8 ns. Distance of the fiber optic hydrophone from the breakdown site is $d = 3$ mm. Each measured point is the average over 50 signals. (Courtesy of O. Lindau).

Measurements of the shock waves from the collapse of a laser induced bubble have been done with a fiber optic hydrophone with a time resolution of less than 5 ns [80, 82]. Figure 18 shows the collapse shock wave form for bubbles of different radii between R_{max} = 0.7 mm and 2.6 mm. The rise time of the pressure pulses is measured to ~15 ns, independent of bubble size. This value must be attributed to the spatial resolution limit of the fiber optic hydrophone due to the diameter of the flat fiber core of 140 μm that intercepts a spherical shock wave. The actual rise time of the shock waves can be expected to attain values below 1 ns (see [83], where a shock front thickness of ~40 nm has been measured for a shock wave of peak pressure 5.8 kbar).

Shock wave amplitudes after plasma formation and bubble collapse are similar (see Fig. 2), but the shapes of the pressure transients differ. During the first collapse phase the pressure rises both within the bubble and in the liquid around the bubble, which is reflected in the 'pedestal' in front of the shock front in Fig. 3 and Fig. 18. The pedestal pressure rises with R_{max} and the (correlated) shock wave strength (Fig. 18).

The shock wave strength (peak pressure of the shock wave) at a distance of 3 mm from the breakdown site perpendicular to the optical axis has been determined as a function of the maximum radius of the bubble and is given in Fig. 19, left diagram. A linearly looking relationship is obtained in the range of maximum bubble radii from about 500 μm to 2.6 mm with the shock wave pressure increasing from ~40 bar to ~210 bar: $p_c \propto R_{max}$. A theoretical investigation [84] gives somewhat lower values with a comparable dependence on R_{max}. The linear curve, however, does not intercepts the origin, but is off by 0.16 mm.

For the same range of bubble radii as the shock wave amplitudes the width of the pressure pulses has been measured (Fig. 19, right diagram). The width increases nonlinearly with R_{max} from 40 ns to 110 ns, the increase being slower for larger bubble radii. No theory has been formulated to describe this dependence.

Streak photographs from the collapse shock wave of laser induced breakdown bubbles are not yet available. Therefore, the maximum pressure at the bubble wall can not be determined by this method. However, the shock wave strength from the hydrophone measurements at some distance from the bubble can be extrapolated down to the minimum bubble radius. When this is done with just taking into account the 1/r spreading for spherical waves and judging the mimimum bubble radius from calculations (compare Fig. 17), the diagram of Fig. 20 is obtained. The collapse pressure values lie in the range of 10 to 25 kbar, a lower limit to the real values. They are about three times lower than the values at breakdown, but the fact that the pressure peaks from breakdown and from bubble collapse are of similar strength when measured for the same event, points to about three times higher values at bubble collapse, i. e., 30 to 75 kbar for maximum bubble radii R_{max} from 500 μm to 3 mm.

So far, spherical and almost spherical bubble collapse has been considered. Then the shock waves are strongest. Aspherical bubble collapse can be induced by boundaries nearby. Figure 21 gives an example, where, because of the complicated, extremely fast sequence of shock wave production, the collapse of a bubble near a flat,

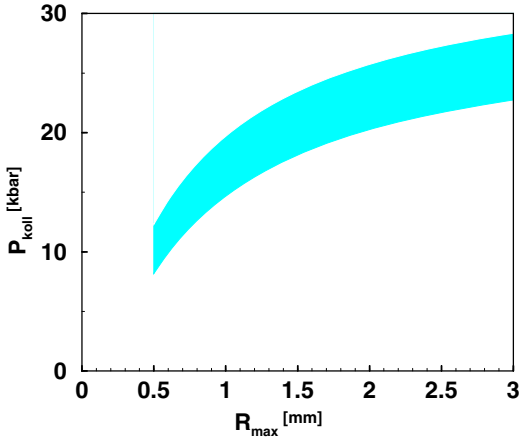

Fig. 20 Collapse of a laser induced bubble in water. First collapse pressure amplitude in dependence on the maximum bubble radius attained after laser induced breakdown extrapolated to the bubble minimum in the acoustic approximation. Nd:YAG laser pulses of width 8 ns. (Courtesy of O. Lindau).

solid boundary has been photographed at 100 million frames per second [80, 79]. An 8 ns Nd:YAG laser pulse has been focused into water at a normalized distance $\gamma = d/R_{\max} = 2.6$, where d is the distance of the breakdown site to the boundary. The bubble collapses in a characteristic way with a high speed liquid jet being developed through the bubble and directed onto the solid boundary (see Fig. 22). The first shock wave occurring has been called "torus shock wave", as it is thought to be generated by the impact of the jet in a spherical contact line on the lower bubble wall due to its larger curvature with respect to the curvature of the lower bubble wall. It is seen in the frames as the two rings to the right and left of the moonlike bubble. Further shock waves are emitted, whose origin has been retraced as given in Fig. 22. No measurements of the shock wave strengths are available for the different types of shock waves occurring at aspherical collapse as it has not been possible to separate the individual contributions of the series of shock waves with a calibrated, sufficiently fast hydrophone.

When a bubble collapses near a boundary, shock wave emission (and other quantities and phenomena as collapse time, jet formation and translatory motion) in water strongly depends on the normalized distance, γ, between bubble center (at breakdown) and the boundary [31]. Pressure pulse measurements have been done at 10 mm distance from the breakdown site with one hydrophone placed above and one aside the bubble. A minimum in acoustic pressure of ~ 20 bar was found at about $\gamma = 0.8$. The pressure rises in an approximately quadratic way between $0.8 < \gamma < 1.5$ to about 150 bar. For $\gamma \to 0$ and for $\gamma \to \infty$ the highest and similar values are obtained (here ~ 250 bar). This becomes clear when considering that for $\gamma \to 0$ the bubble approaches a hemispherical shape and for $\gamma \to \infty$ it retains its spherical shape, both forms leading to a similar collapse.

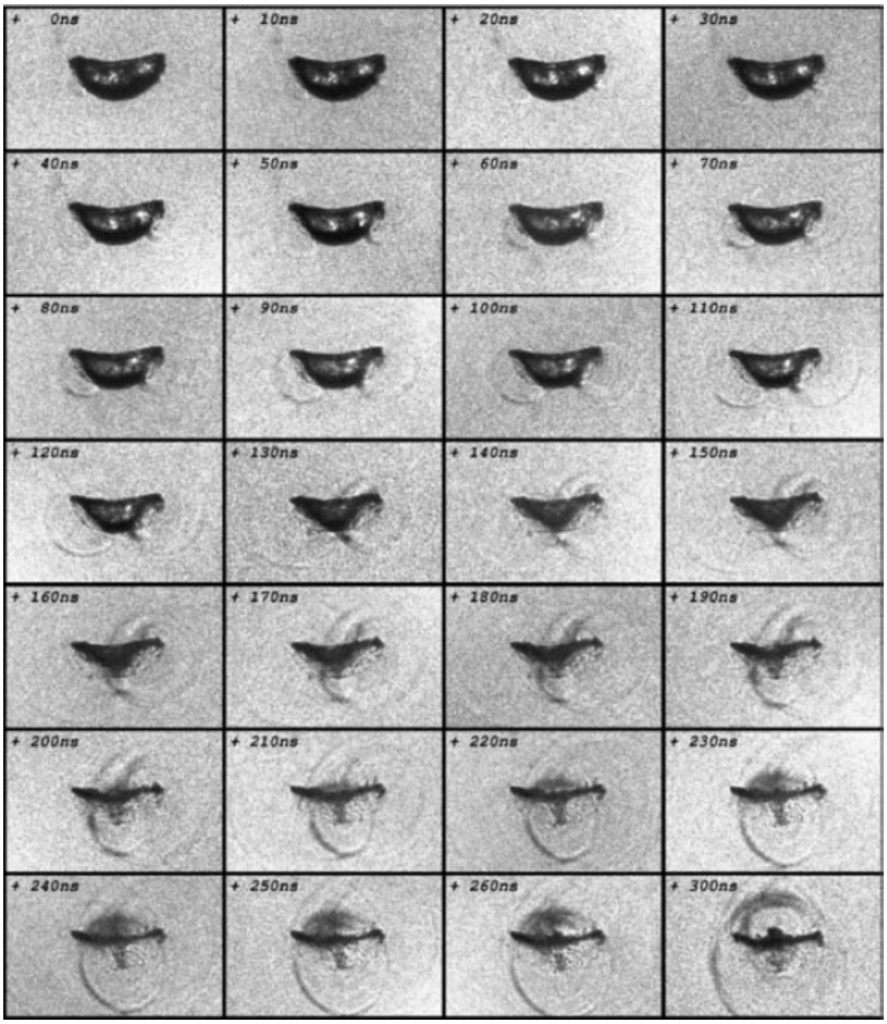

Fig. 21 Collapse of a laser induced bubble in water near a plane, solid surface. Nd:YAG laser pulse of width 8 ns. Interframe time 10 ns, between the last two frames 40 ns. Maximum bubble radius $R_{\max} = 1.5$ mm, $\gamma = 2.6$. Picture size (height $\times$ width) = 0.8 $\times$ 1.3 mm. (Courtesy of O. Lindau).

Laser induced bubbles and shock waves can also be generated near a free surface (where the liquid is free to move and not constrained as in the case of a solid surface) and also near compliant surfaces with properties in between these two limiting cases [85, 86]. An example of bubble dynamics and the series of shock waves emitted are given in Fig. 23 for an elastic boundary (polyacrylamide with 80 % water content) with the stand-off parameter being $\gamma = 0.62$ [85]. The final phase of bubble collapse and the first phase of bubble rebound are shown with three different

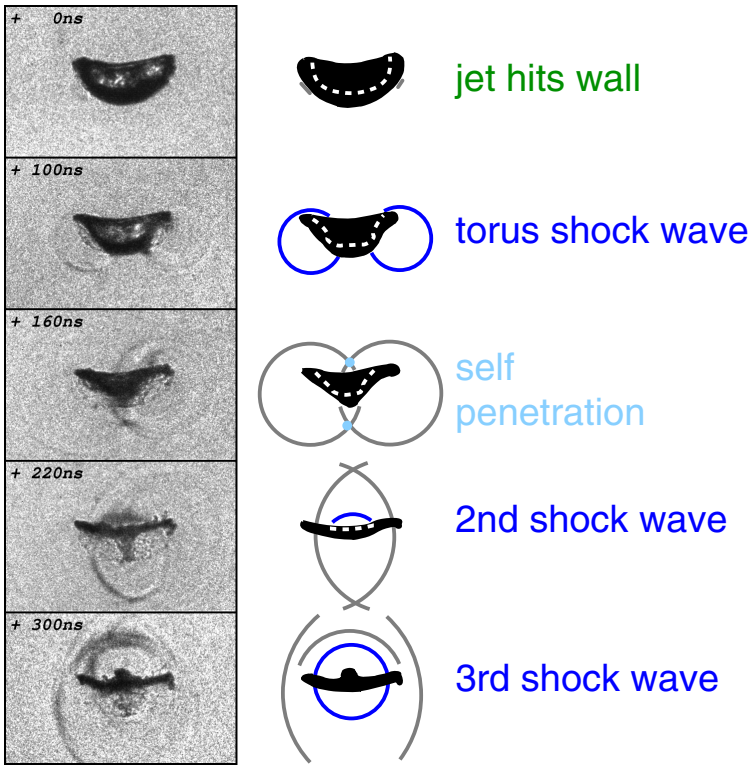

Fig. 22 Collapse of a laser induced bubble in water near a plane, solid surface. Nd:YAG laser pulse of width 8 ns. Maximum bubble radius $R_{\max} = 1.5$ mm, $\gamma = 2.6$. Picture size (height $\times$ width) = 0.8 $\times$ 1.3 mm. Explanation of the various shock waves emitted. (Courtesy of O. Lindau).

time resolutions. The upper row of Fig. 23 gives an overview of bubble dynamics with the characteristic bubble deformation to a mushroom shape, subsequent bubble splitting and the development of two (high velocity) jets in opposite directions, one entering the elastic sample. An enlargement both in space and time is given in the middle row. The time resolution has been increased by a factor of 20 using one million frames per second and the spatial resolution has been increased by a factor of 2.5. The eight frames comprise a time interval between frame 5 and frame 6 of the upper row of Fig. 23, when the bubble is in its collapse and rebound phase. A disintegration of the bubble is observed. For more details and for observing the shock waves, the time resolution has been increased further to five million frames per second (lower row). The series starts, when the annular inflow of water parallel to the boundary almost closes on the bubble axis (perpendicular to the boundary) splitting the bubble. The closure point on the bubble axis is asymmetric leaving a larger volume of gas and vapor near the boundary and squeezing the liquid in opposite directions, toward the boundary and away from it, leading to a jet each through

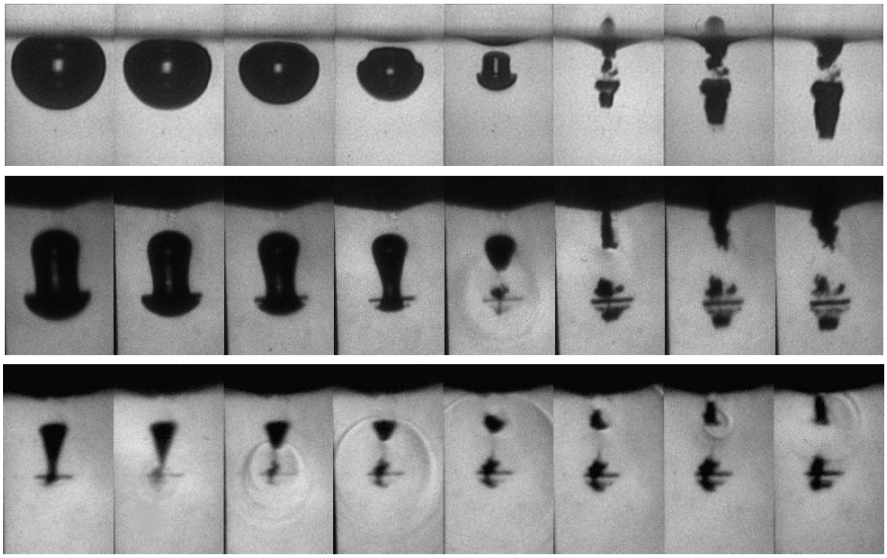

Fig. 23 Final phase of the bubble collapse in water and the first phase of rebound near an elastic boundary with $\gamma = 0.62$, $R_{max} = 1.55$ mm. Q-switched Nd:YAG laser pulse. 50 000 frames per second, frame width 3.5 mm (upper row); one million frames per scond, frame width 1.4 mm (middle row); five million frames per second, frame width 1.4 mm (lower row) [85].

the interior of the respective bubble part. Shock waves are emitted upon closure of the annular jet on the bubble axis the emission center running with the separating closure point along the axis. Almost simultaneously with the closure of the annular jet, the bubble cap collapses and emits a shock wave. It runs with the annular jet driven shocks towards the lower larger bubble part helping in its compression. This leads to a particularly high velocity jet towards the elastic boundary, even penetrating it as seen in frames 6 and 7 of the upper row of Fig. 23. When this jet hits the bubble wall near the boundary, a shock wave is emitted. Later, a further shock wave is emitted, when the lower bubble part collapses. The velocity of this high speed jet has been determined to 960 m/s. Shock wave strengths have not yet been measured.

6 Applications and Future Perspectives

Laser induced bubbles and their shock waves have found application in cavitation research (see [11, 26, 27, 28, 87, 88, 89, 90, 91, 92] and the reviews [72, 73]), inertial confinement fusion research [93, 94], wet laser cleaning [95, 96], pulsed laser ablation in water and biological tissue [97, 98], laser lithotripsy [34, 99, 100, 101, 102], photodisruption [30, 103, 42, 104], laser-induced cell lysis [105, 106, 107, 108], micro- and nanosurgery [59, 39, 109, 67], and gene transfection [110,

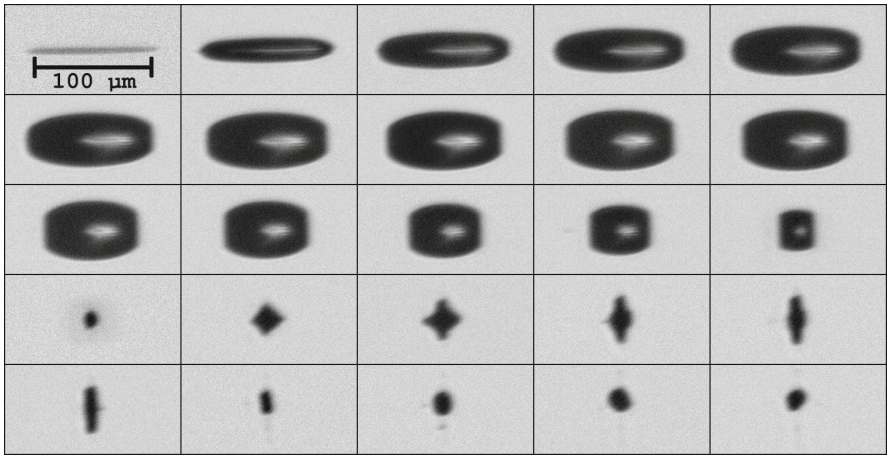

Fig. 24 Femtosecond laser induced bubble dynamics in water. Ti:Sapphire laser of wavelength 810 nm and pulse width 130 fs. Laser energy per pulse 800 nJ. Interframe time 400 ns. (Courtesy of R. Geisler).

111]. Laser induced bubbles have also stimulated and stimulate the improvement of measurement techniques [112] and of theory [84, 113, 114]. Some of these areas will be discussed below.

In cavitation research, laser induced breakdown has made possible systematic investigations into the behavior of bubbles, small or large, either in the bulk of liquids or near boundaries of various kinds (solid, flexible, free), either spherical or aspherical (see the reviews [72, 73]). Just one example from this large area is given in Fig. 24, where the elongated breakdown from a femtosecond laser pulse and its dynamics are shown. A cylindrical breakdown plasma is formed developing into an elliptical bubble that lateron undergoes a metamorphosis to a multitude of different shapes from can shaped to almost spherical, diamond shaped, star like and disk shaped. A cylindrical shock wave is emitted upon breakdown of the femtosecond laser pulse of duration 130 fs. No detailed measurements, however, are known concerning the strength and width of these pressure waves. Figure 25 shows the cylindrical breakdown shock wave and the spherical collapse shock wave from a femtosecond laser pulse focused into water [115]. The shock waves have been recorded under backlight conditions with a femtosecond laser pulse of duration 85 fs to stop the motion of the shock waves. The upper and lower dark lines are from the cylindrical shock wave, the dark line in the middle is the shadow from the emerging elliptical bubble 60 ns after breakdown. The bubble develops as in Fig. 24 and collapses almost spherically with the emission of a spherical shock wave shown in Fig. 25 at the time instant 7.8 μs after breakdown. Controlled elongated optical breakdown is reported by Toytman et al. [116] for a 1 ps laser pulse focused into water by an axicon–lens combination. They recommend elongated breakdown for linear and planar dissection of transparent media and ophthalmic surgical applications, for instance cataract surgery. The advantage of this method is that it can be

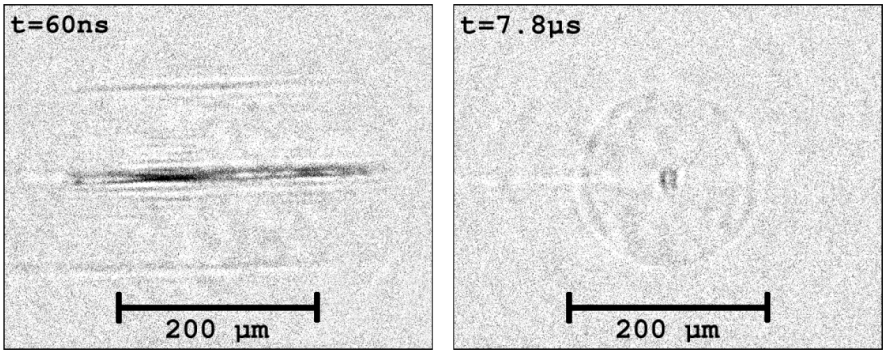

Fig. 25 Laser induced cylindrical shock wave after focusing a fs-laser pulse into water (left) and spherical shock wave after spherical collapse of the initially thin elliptical bubble produced (right). Ti:Sapphire laser of wavelength 810 nm and pulse width 130 fs. Laser energy per pulse 8 μJ. Exposure time 85 fs. (Courtesy of R. Geisler).

applied to any duration of laser pulses and is not restricted to femtosecond pulses with their self-focusing properties [117].

Laser induced shock waves have been used to compress small bubbles [92] as a model to phenomena occurring in various branches of science and technology, for instance in shock wave lithotripsy or shock wave cleaning. In [92], a hydrophone recording of a laser induced breakdown shock wave taken with an optical hydrophone [58] can be found as well as several photographic sequences of laser shock wave induced bubble dynamics in different fluid flow geometries (single wall, cleft of a solid surface, between walls, multiple bubbles). A multitude of phenomena is observed after shock wave passage including jet formation, toroidal bubbles, surface instabilities with daughter bubble formation, bubble migration, multiple jet formation in multi-wall geometries (jet competition), splitting, merging and agglomeration of bubbles as well as cleaving of particles. Many more experiments can be conceived in this direction.

Inertial confinement fusion wants to make use of the huge compression ratios that can be achieved in spherical geometry and the high temperatures that should occur (see, for instance, [94], where an idealised spherical compression from a converging shock wave is calculated and a scheme for the compression of a deuterium–tritium (DT) gas bubble is proposed). However, shape instabilities arising upon collapse of spherical bubbles (DT gas mixture or other) prevent reaching thermonuclear burn (see the calculations on bubble shape stability in the final run away collapse phase of a bubble [64]).

The cleaning of surfaces from contaminations is of great importance in many areas, in particular the chip industry that is in need of extremely clean surfaces of their wafers. In this respect, the cleaning with laser induced bubbles and their shock waves has been suggested called “wet laser cleaning” [95]. A bubble is produced in the liquid near the submerged surface to be cleaned and the jet and the collapse shock wave are thought to be the agents to remove the contaminations from the

surface in a mild action below erosion [88, 89, 90]. This has been elucidated further in high speed photographic investigations by determining the time when the contamination particles are set into motion on the surface in relation to the bubble dynamics [96]. It was found that the particles are transported radially away with the jet flow from the jet impact site on the surface.

An application of laser pulses, where strong shock waves occur, is irradiating absorbing objects under water or a liquid surface with high (linear) absorption of the laser light used. Then material is ejected, a phenomenon called laser ablation (see the review [97]). Subsurface peak pressures in water of 9.3 kbar have been measured after irradiating the water surface with 70 ns pulses of an Er:YAG laser (wavelength 2.94 nm) at an exposure of 5.4 J/cm^2 [98]. Bubbles come into play, when the absorbing material is submerged in a transparent liquid and the energy supplied, often by an optical fiber, then is confined by the inertia of the surrounding liquid. Bubble formation adds to the complexity of the phenomena and may cause collateral damage in tissue ablation due to bubble expansion and its collapse shock wave [97, 103]. However, when used in laser lithotripsy, these side effects add in the destruction of the stone, in particular for long laser pulses (microsecond range) [99]. It has been found that in the case of microsecond laser pulses from flashlamp pumped dye lasers the laser breakdown pressure is far less than the first bubble collapse pressure [100]. It is argued that it is this bubble collapse pressure that destructs stones in dye laser lithotripter applications [99]. Experiments with simultaneously observing the laser induced bubble formed and the shock waves emitted confirm this interpretation [102]. For holmium lithotripsy with its long wavelength of 2100 nm and long pulses of 250 to 350 μs, a different mechanism for stone fragmentation is suggested, as the bubbles produced are irregular in shape and give only small collapse pressures. Instead, the long laser pulse forms a vapor channel to the stone and causes thermal ablation [102]. As the optical delivery fiber itself is prone to destruction from bubble collapse, ultrasonic stone destruction methods gain thrust as an alternative.

Laser induced breakdown may be used for rapid cell lysis, for instance for cell bioanalytics. Although laser microbeams (laser beams with large focusing angle) are widely used for this purpose, the processes of laser–cell interaction leading to cell disruption are not well understood. Plasma formation, shock wave emission and bubble dynamics are all candidates for cell lysis. Time resolved experiments have been conducted by Rau et al. [105, 106] to decide on this question (Fig. 26). Laser induced breakdown was effected 10 μm above a monolayer of cells at three times the breakdown threshold with a (532 nm, 6 ns, 24 μJ) Nd:YAG laser pulse and recorded with different time delays at a later instant. The plasma is typically gone after 25–30 ns. Here, the plasma luminescence is to be seen in Fig. 26 (a) and (b). The breakdown shock wave is seen in Fig. 26 (a), (b), (c) and is out of sight in (d). A bubble develops and expands. Whereas the shock wave seems to do no harm to the cells, the expanding bubble squeezes the liquid between the breakdown site and cell monolayer radially outward exerting strong stresses on the cells lysing them up to a certain radius. This is best seen in the image Fig. 26 (i) as the innermost area. This area is later cleaned from cell debris by the bubble jet known to develop upon bubble collapse in a comparable situation [14, 12] (see Fig. 26 (l)). When the

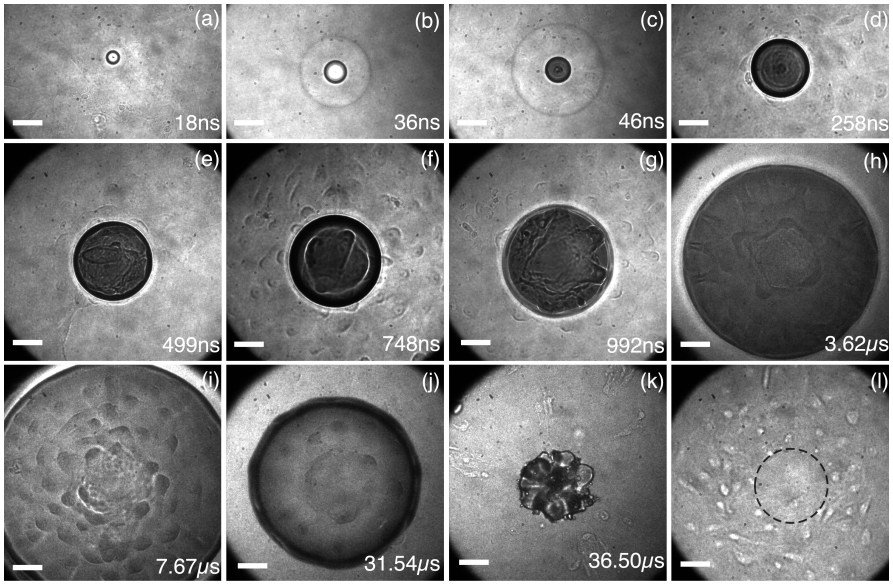

Fig. 26 Time resolved image series of cell lysis. (a) to (k) images taken at the indicated time after breakdown. (l) phase contrast image after the laser pulse. $\gamma = 0.06 - 0.13$. Q-switched, frequency-doubled Nd:YAG laser pulse, wavelength 532 nm, pulse width 6 ns, pulse energy 24 μJ (3 times the breakdown threshold). Distance to the cell monolayer 10 μm. 1000 cells/mm^2. Scale bar = 50 μm. (Courtesy of V. Venugopalan [106]).

breakdown site is set to 400 μm, corresponding to $\gamma = 1.6$ at three times the breakdown threshold, it is the jet that leads to cell lysis, not the bubble expansion. From laser induced cavitation bubble erosion experiments it is known that the erosion potential and erosion patterns strongly depend on the (normalized) distance of the bubble to the boundary [89, 90].

Acknowledgements. The authors thank the numerous coworkers who helped in collecting the material and results presented in the overview, in particular T. Kurz, R. Geisler, O. Lindau, C. D. Ohl, D. Kröninger, E.-A. Brujan, S. Busch, K. Nahen and J. Noack.

References

1. Askar'yan, G.A., Prokhorov, A.M., Chanturiya, I.F., Shipulo, G.P.: The effects of a laser beam in a liquid. Sov. Phys. – JETP 17, 1463–1465 (1963)
2. Brewer, R.G., Rieckhoff, K.E.: Stimulated Brillouin scattering in liquids. Phys. Rev. Lett. 13, 334–336 (1964)
3. Carome, E.F., Moeller, C.E., Clark, N.A.: Intense ruby-laser-induced acoustic impulses in liquids. J. Acoust. Soc. Am. 40, 1462–1466 (1966)

4. Bell, C.E., Landt, J.A.: Laser-induced high-pressure shock waves in water. Appl. Phys. Lett. 10, 46–48 (1967)
5. Carome, E.F., Carreira, E.M., Prochaska, C.J.: Photographic studies of laser-induced pressure impulses in liquids. Appl. Phys. Lett. 11, 64–66 (1967)
6. Barnes, P.A., Rieckhoff, K.E.: Laser induced underwater sparks. Appl. Phys. Lett. 13, 282–284 (1968)
7. Felix, M.P., Ellis, A.T.: Laser-induced liquid breakdown – a step-by-step account. Appl. Phys. Lett. 19, 484–486 (1971)
8. Buzukov, A.A., Teslenko, V.S.: Sonoluminescence following of focusing laser radiation into a liquid. J. Exp. Theor. Phys. Lett. 14, 189–191 (1971)
9. Lauterborn, W.: High-speed photography of laser-induced breakdown in liquids. Appl. Phys. Lett. 21, 27–29 (1972)
10. Akmanov, A.G., Ben'kovskii, V.G., Golubnichii, P.I., Maslennikov, S.I., Shemanin, V.G.: Laser sonoluminescence in a liquid. Sov. Phys. Acoust. 19, 417–418 (1974)
11. Lauterborn, W.: Kavitation durch Laserlicht (Cavitation by laser light). Acustica 31, 51–78 (1974) (in German)
12. Lauterborn, W., Bolle, H.: Experimental investigations of cavitation-bubble collapse in the neighbourhood of a solid boundary. J. Fluid Mech. 72, 391–399 (1975)
13. Lauterborn, W., Ebeling, K.J.: High-speed holography of laser-induced breakdown in liquids. Appl. Phys. Lett. 31, 663–664 (1977)
14. Plesset, M.S., Chapman, R.B.: Collapse of an initially spherical vapour cavity in the neighbourhood of a solid boundary. J. Fluid Mech. 47, 283–290 (1971)
15. Teslenko, V.S.: Investigation of photoacoustic and photohydrodynamic parameters of laser induced breakdown in liquids. Kvantovaya Electronica 4, 1732–1737 (1977) (in Russian); Tranlation in: Sov. J. Quantum Electr. 7, 981–984 (1977)
16. Ebeling, K.J.: Zum Verhalten kugelförmiger, lasererzeugter Kavitationsblasen in Wasser (The behavior of spherical laser-produced bubbles in water). Acustica 40, 229–239 (1978) (in German)
17. Lauterborn, W. (ed.): Cavitation and Inhomogeneities in Underwater Acoustics. Springer, Heidelberg (1980)
18. Lauterborn, W.: Cavitation and coherent optics. In: [17], pp. 3–12 (1980)
19. V. S. Teslenko: Experimental investigation of bubble collapse at laser-induced breakdown in liquids. In: [17], pp. 30–34 (1980)
20. Ebeling, K.J.: Application of high speed holocinematographical methods in cavitation research. In: [17], pp. 35–41 (1980)
21. Lauterborn, W., Timm, R.: Bubble collapse studies at a million frames per second. In: [17], pp. 42–46 (1980)
22. Hentschel, W., Lauterborn, W.: Holographic generation of multi-bubble systems. In: [17], pp. 47–53 (1980)
23. Hentschel, W., Lauterborn, W.: Acoustic emission of single laser-produced cavitation bubbles and their dynamics. Appl. Scient. Res. 38, 225–230 (1982)
24. Lauterborn, W., Hentschel, W.: Cavitation bubble dynamics studied by high speed photography and holography: part one. Ultrasonics 23, 260–268 (1985)
25. Lauterborn, W., Hentschel, W.: Cavitation bubble dynamics studied by high speed photography and holography: part two. Ultrasonics 24, 59–65 (1986)
26. Shima, A., Takayama, K., Tomita, Y., Miura, N.: An experimental study on effects of a solid wall on the motion of bubbles and shock waves in bubble collapse. Acustica 48, 293–301 (1981)
27. Tomita, Y., Shima, A.: Mechanisms of impulsive pressure generation and damage pit formation by bubble collapse. J. Fluid Mech. 169, 535–564 (1986)

28. Shima, A., Tomita, Y., Gibson, D.C., Blake, J.R.: The growth and collapse of cavitation bubbles near composite surfaces. J. Fluid Mech. 203, 199–214 (1989)
29. Fujimoto, J.G., Lin, W.Z., Ippen, E.P., Puliafito, C.A., Steinert, R.F.: Time-resolved studies of Nd:YAG laser-induced breakdown - Plasma formation, acoustic wave generation, and cavitation. Invest. Ophthalmol. Vis. Sci. 26, 1771–1777 (1985)
30. Vogel, A., Hentschel, W., Holzfuss, J., Lauterborn, W.: Cavitation bubble dynamics and acoustic transient generation in ocular surgery with pulsed neodymium:YAG lasers. Ophthalmology 93, 1259–1269 (1986)
31. Vogel, A., Lauterborn, W.: Acoustic transient generation by laser-produced cavitation bubbles near solid boundaries. J. Acoust. Soc. Am. 84, 719–731 (1988)
32. Vogel, A., Lauterborn, W., Timm, R.: Optical and acoustical investigations of the dynamics of laser-produced cavitation bubbles near a solid boundary. J. Fluid Mech. 206, 299–338 (1989)
33. Zysset, B., Fujimoto, J.G., Deutsch, T.F.: Time resolved measurements of picosecond optical breakdown. Appl. Phys. B 48, 139–147 (1989)
34. Teng, P., Nishioka, N.S., Anderson, R.R., Deutsch, T.F.: Optical studies of pulsed-laser fragmentation of biliary calculi. Appl. Phys. B 42, 73–78 (1987)
35. Hickling, R., Plesset, M.S.: Collapse and rebound of a spherical bubble in water. Phys. Fluids 7, 7–14 (1964)
36. Fujikawa, S., Akamatsu, T.: Effects of the non-equilibrium condensation of vapour on the pressure wave produced by the collapse of a bubble in a liquid. J. Fluid Mech. 97, 481–512 (1980)
37. Kennedy, P.K., Hammer, D.X., Rockwell, B.A.: Laser-induced breakdown in aqueous media. Prog. Quantum Electr. 21, 155–248 (1997)
38. Noack, J., Vogel, A.: Laser-induced plasma formation in water at nanosecond to femtosecond time scales: Calculation of thresholds, absorption coefficients, and energy density. IEEE J. Quantum Electr. 35, 1156–1167 (1999)
39. Vogel, A., Noack, J., Hüttmann, G., Paltauf, G.: Mechanism of femtosecond laser nanosurgery of cells and tissues. Appl. Phys. B 81, 1015–1047 (2005)
40. Williams, F., Varma, S.P., Hillenius, S.: Liquid water as a lone-pair amorphous semiconductor. J. Chem. Phys. 64, 1549–1554 (1976)
41. Sacchi, C.A.: Laser-induced electric breakdown in water. J. Opt. Soc. Am. B 8, 337–344 (1991)
42. Vogel, A., Busch, S., Jungnickel, K., Birngruber, R.: Mechanisms of intraocular photodisruption with picosecond and nanosecond laser pulses. Lasers Surg. Med. 15, 32–43 (1994)
43. Vogel, A., Nahen, K., Theisen, D., Noack, J.: Plasma formation in water by picosecond and nanosecond Nd:YAG laser pulses – Part I: Optical breakdown at threshold and superthreshold irradiance. IEEE J. Sel. Top. Quantum Electr. 2, 847–860 (1996)
44. Toker, G., Bulatov, V., Kovalchuk, T., Schechter, I.: Micro-dynamics of optical breakdown in water induced by nanosecond laser pulses of 1064 nm wavelength. Chem. Phys. Lett. 471, 244–248 (2009)
45. Vogel, A., Busch, S., Parlitz, U.: Shock wave emission and cavitation bubble generation by picosecond and nanosecond optical breakdown in water. J. Acoust. Soc. Am. 100, 148–165 (1996)
46. Noack, J., Vogel, A.: Single-shot spatially resolved characterization of laser-induced shock waves in water. Appl. Opt. 37, 4092–4099 (1998)
47. Kudryashov, S.I., Zvorykin, V.D.: Microscale nanosecond laser-induced optical breakdown in water. Phys. Rev. E 78, 036404 (2008)

48. Byun, K.T., Kwak, H.Y.: A model of laser-induced cavitation. Jpn. J. Appl. Phys. 43, 621–630 (2004)
49. Noack, J., Hammer, D.X., Noojin, G.D., Rockwell, B.A., Vogel, A.: Influence of pulse duration on mechanical effects after laser-induced breakdown in water. J. Appl. Phys. 83, 7488–7495 (1998)
50. Hentschel, W., Lauterborn, W.: High-speed holographic movie camera. Opt. Engineering 24, 687–691 (1985)
51. Quinto-Su, P.A., Venugopalan, V., Ohl, C.D.: Generation of laser-induced cavitation bubbles with a digital hologram. Opt. Express 16, 18964–18969 (2008)
52. Lim, K.Y., Quinto-Su, P.A., Klaseboer, E., Khoo, B.C., Venugopalan, V., Ohl, C.D.: Nonspherical laser-induced cavitation bubbles. Phys. Rev. E 81, 016308-1–016308-9 (2010)
53. Jayasinghe, A.K., Rohner, J., Hutson, M.S.: Holographic UV laser microsurgery. Biomed. Opt. Express 2, 2590–2598 (2011)
54. Docchio, F., Regondi, P., Capon, M.R.C., Mellerio, J.: Study of the temporal and spatial dymanics of plasmas induced in liquids by nanosecond Nd:YAG laser pulses. 1: Analysis of the plasma starting times. Appl. Opt. 27, 3661–3668 (1988)
55. Juhasz, T., Kastis, G.A., Suárez, C., Bor, Z., Bron, W.E.: Time-resolved observations of shock waves and cavitation bubbles generated by femtosecond laser pulses in corneal tissue and water. Lasers Surg. Med. 19, 23–31 (1996)
56. Schaffer, C.B., Nishimura, N., Glezer, E.N., Kim, A.M.-T., Mazur, E.: Dynamics of femtosecond laser-induced breakdown in water from femtoseconds to microseconds. Opt. Express 10, 196–203 (2002)
57. Vogel, A., Noack, J., Nahen, K., Theisen, D., Busch, S., Parlitz, U., Hammer, D.X., Noojin, G.D., Rockwell, B.A., Birngruber, R.: Energy balance of optical breakdown in water at nanosecond to femtosecond time scales. Appl. Phys. B 68, 271–280 (1999)
58. Staudenraus, J., Eisenmenger, W.: Fibre-optic probe hydrophone for ultrasonic and shock-wave measurements in water. Ultrasonics 31, 267–273 (1993)
59. Venugopalan, V., Guerra III, A., Nahen, K., Vogel, A.: Role of laser-induced plasma formation in pulsed cellular microsurgery and micromanipulation. Phys. Rev. Lett. 88, 078103 (2002)
60. Rice, M.H., Walsh, J.M.: Equation of state of water to 250 kilobars. J. Chem. Phys. 26, 824–830 (1957)
61. Brujan, E.A., Vogel, A.: Stress wave emission and cavitation bubble dynamics by nanosecond optical breakdown in a tissue phantom. J. Fluid Mech. 558, 281–308 (2006)
62. Ohl, C.D., Lindau, O., Lauterborn, W.: Luminescence from spherically and aspherically collapsing laser induced bubbles. Phys. Rev. Lett. 80, 393–396 (1998)
63. Kröninger, D., Köhler, K., Kurz, T., Lauterborn, W.: Particle tracking velocimetry of the flow field around a collapsing cavitation bubble. Exp. Fluids 48, 395–408 (2010)
64. Strube, H.W.: Numerische Untersuchungen zur Stabilität nichtsphärisch schwingender Blasen (Numerical investigations on the stability of nonspherically oscillating bubbles). Acustica 25, 289–303 (1971)
65. Rayleigh, L.: On the pressure developed in a liquid during the collapse of a spherical cavity. Phil. Mag. Ser. 6 34, 94–98 (1917)
66. Lauterborn, W.: Eigenfrequenzen von Gasblasen in Flüssigkeiten (Natural frequencies of gas bubbles in liquids). Acustica 20, 14–20 (1968)
67. Vogel, A., Linz, N., Freidank, A., Paltauf, G.: Femtosecond-laser-induced nanocavitation in water: Implications for optical breakdown thresholds and cell surgery. Phys. Rev. Lett. 100, 038102 (2008)

68. Baghdassarian, O., Tabbert, B., Williams, G.A.: Luminescence characteristics of laser-induced bubbles in water. Phys. Rev. Lett. 83, 2437–2440 (1999)
69. Gilmore, F.R.: The growth or collapse of a spherical bubble in a viscous compressible liquid. Report No. 26-4, Hydrodynamics Laboratory, California Institute of Technology, Pasadena, California, USA (1952)
70. Löfstedt, R., Barber, B.P., Putterman, S.J.: Toward a hydrodynamic theory of sonoluminescence. Phys. Fluids A 5, 2911–2928 (1993)
71. Brennen, C.E.: Cavitation and Bubble Dynamics. Oxford University Press, New York (1995)
72. Lauterborn, W., Kurz, T., Mettin, R., Ohl, C.D.: Experimental and theoretical bubble dynamics. Adv. Chem. Phys. 110, 295–380 (1999)
73. Lauterborn, W., Kurz, T.: Physics of bubble oscillations. Rep. Prog. Phys. 73, 106501-1–106501-88 (2010)
74. Keller, J.B., Miksis, M.: Bubble oscillations of large amplitude. J. Acoust. Soc. Am. 68, 628–633 (1980)
75. Lauterborn, W., Parlitz, U.: Methods of chaos physics and their applications to acoustics. J. Acoust. Soc. Am. 84, 1975–1993 (1988)
76. Parlitz, U., Englisch, V., Scheffczyk, C., Lauterborn, W.: Bifurcation structure of bubble oscillators. J. Acoust. Soc. Am. 88, 1061–1077 (1990)
77. Prosperetti, A., Lezzi, A.: Bubble dynamics in a compressible liquid. Part 1. First-order theory. J. Fluid Mech. 168, 457–478 (1986)
78. Lezzi, A., Prosperetti, A.: Bubble dynamics in a compressible liquid. Part 2. Second-order theory. J. Fluid Mech. 185, 289–321 (1987)
79. Lindau, O., Lauterborn, W.: Cinematographic observation of the collapse and rebound of a laser-produced cavitation bubble near a wall. J. Fluid Mech. 479, 327–348 (2003)
80. Lindau, O.: Untersuchungen zur lasererzeugten Kavitation (Investigation of laser induced cavitation). Der Andere Verlag, Osnabrück (2001)
81. Fuster, D., Dopazo, C., Hauke, G.: Liquid compressibility effects during the collapse of a single cavitating bubble. J. Acoust. Soc. Am. 129, 122–131 (2011)
82. Lauterborn, W., Kurz, T., Geisler, R., Schanz, D., Lindau, O.: Acoustic cavitation, bubble dynamics and sonoluminescence. Ultrason. Sonochem. 14, 484–491 (2007)
83. Harris, P., Presles, H.N.: Reflectivity of a 5.8 kbar schock front in water. J. Chem. Phys. 74, 6864–6866 (1981)
84. Akhatov, I., Lindau, O., Topolnikov, A., Mettin, R., Vakhitova, A., Lauterborn, W.: Collapse and rebound of a laser-induced cavitation bubble. Phys. Fluids 13, 2805–2819 (2001)
85. Brujan, E.A., Nahen, K., Schmidt, P., Vogel, A.: Dynamics of laser-induced cavitation bubbles near an elastic boundary. J. Fluid Mech. 433, 251–281 (2001)
86. Brujan, E.A., Nahen, K., Schmidt, P., Vogel, A.: Dynamics of laser-induced cavitation bubbles near elastic boundaries: influence of the elastic modulus. J. Fluid Mech. 433, 283–314 (2001)
87. Tomita, Y., Shima, A.: High-speed photographic observations of laser-induced cavitation bubbles in water. Acustica 71, 161–171 (1990)
88. Philipp, A., Lauterborn, W.: Damage of solid surfaces by single laser-produced cavitation bubbles. Acustica · Acta Acustica 83, 223–227 (1997)
89. Isselin, J.-C., Alloncle, A.-P., Autric, M.: On laser induced single bubble near a solid boundary: Contribution to the understanding of erosion phenomena. J. Appl. Phys. 84, 5766–5771 (1998)
90. Philipp, A., Lauterborn, W.: Cavitation erosion by single laser-produced bubbles. J. Fluid Mech. 361, 75–116 (1998)

91. Shaw, S.J., Schiffers, W.P., Gentry, T.P., Emmony, D.C.: A study of the interaction of a laser-generated cavity with a nearby solid boundary. J. Phys. D: Appl. Phys. 32, 1612–1617 (1999)
92. Wolfrum, B., Kurz, T., Mettin, R., Lauterborn, W.: Shock wave induced interaction of microbubbles and boundaries. Phys. Fluids 15, 2916–2922 (2003)
93. Geisler, R., Schmidt-Ott, W.D., Kurz, T., Lauterborn, W.: Search for neutron emission in laser-induced cavitation. Europhys. Lett. 66, 435–440 (2004)
94. Grinenko, A., Gurovich, V.T., Krasik, Y.E.: Implosion in water medium and its possible application for the inertial confinement fusion target ignition. Phys. Plasmas 14, 12701-1–12701-7 (2007)
95. Song, W.D., Hong, M.H., Lukyanchuk, B., Chong, T.C.: Laser-induced cavitation bubbles for cleaning of solid surfaces. J. Appl. Phys. 95, 2952–2956 (2004)
96. Ohl, C.D., Arora, M., Dijkink, R., Janve, V., Lohse, D.: Surface cleaning from laser-induced cavitation bubbles. Appl. Phys. Lett. 89, 074102-1–074102-3 (2006)
97. Vogel, A., Venugopalan, V.: Mechanisms of pulsed laser ablation of biological tissue. Chem. Rev. 103, 577–644 (2003)
98. Apitz, I., Vogel, A.: Material ejection in nanosecond Er:YAG laser ablation of water, liver, and skin. Appl. Phys. A 81, 329–338 (2005)
99. Rink, K., Delacrétaz, G., Salathé, R.P.: Fragmentation process induced by microsecond laser pulses during lithotripsy. Appl. Phys. Lett. 61, 258–260 (1992)
100. Rink, K., Delacrétaz, G., Salathé, R.P.: Fragmentation process of current laser lithotripters. Lasers Surg. Med. 16, 134–146 (1995)
101. Vogel, A.: Nonlinear absorption: intraocular microsurgery and laser lithotripsy. Phys. Med. Biol. 42, 895–912 (1997)
102. Zhong, P., Tong, H.L., Cocks, F.H., Pearle, M.S., Preminger, G.M.: Transient cavitation and acoustic emission produced by different laser lithotripters. J. Endourol. 12, 371–378 (1998)
103. Vogel, A., Schweiger, P., Frieser, A., Asiyo, M.A., Birngruber, R.: Intraocular Nd:YAG laser surgery: Light-tissue interaction, damage range, and reduction of collateral effects. IEEE J. Quantum Electr. 26, 2240–2260 (1990)
104. Vogel, A., Capon, M.R.C., Asiyo-Vogel, A.N., Birngruber, R.: Intraocular Photodisruption with picosecond and nanosecond laser pulses: Tissue effects in cornea, lens, and retina. Invest. Ophthalm. Vis. Sci. 35, 3032–3044 (1994)
105. Rau, K.R., Guerra III, A., Vogel, A., Venugopalan, V.: Investigation of laser-induced cell lysis using time resolved imaging. Appl. Phys. Lett. 84, 2940–2942 (2004)
106. Rau, K.R., Quinto-Su, P.A., Hellman, A.N., Venugopalan, V.: Pulsed laser microbeam-induced cell lysis: Time-resolved imaging and analysis of hydrodynamic effects. Biophys. J. 91, 317–329 (2006)
107. Quinto-Su, P.A., Lai, H.H., Yoon, H.H., Sims, C.E., Allbritton, N.L., Venugopalan, V.: Examination of laser microbeam cell lysis in a PDMS microfluidic channel using time-resolved imaging. Lab Chip 8, 408–414 (2008)
108. Hellman, A.N., Rau, K.R., Yoon, H.H., Venugopalan, V.: Biophysical response to pulsed laser microbeam-induced cell lysis and molecular delivery. J. Biophoton 1, 24–35 (2008)
109. Hutson, M.S., Ma, X.: Plasma and cavitation dynamics during pulsed laser microsurgery *in vivo*. Phys. Rev. Lett. 99, 158104 (2007)
110. Stevenson, D.J., Gunn-Moore, F.J., Campbell, P., Dholakia, K.: Single cell optical transfection. J. R. Soc. Interface 7, 863–871 (2010)
111. Arita, Y., Torres-Mapa, M.L., Lee, W.M., Čišmár, T., Campbell, P., Gunn-Moore, F.J., Dholakia, K.: Spatially optimized gene transfection by laser-induced breakdown of optically trapped nanoparticles. Appl. Phys. Lett. 98, 093702-1–093702-3 (2011)

112. Hendijanifard, M., Willis, D.A.: An improved method to experimentally determine temperature and pressure behind laser-induced shock waves at low Mach numbers. J. Phys. D: Appl. Phys. 44, 145501-1–145501-6 (2011)
113. Müller, S., Bachmann, M., Kröninger, D., Kurz, T., Helluy, P.: Comparison and validation of compressible flow simulations of laser-induced bubbles. Comp. Fluids 38, 1850–1862 (2009)
114. Müller, S., Helluy, P., Ballmann, J.: Numerical simulation of a single bubble by compressible two-phase fluids. Int. J. Numer. Meth. Fluids 62, 591–631 (2010)
115. Geisler, R.: Untersuchungen zur laserinduzierten Kavitation mit Nanosekunden- und Femtosekundenlasern (Investigation of laser-induced cavitation with nanosecond and femtosecond lasers). Dissertation, University of Göttingen (2003) Universitätsverlag, Göttingen (2004) ISBN 3-930457-38-5
116. Toytman, I., Simanovski, D., Palanker, D.: Optical breakdown in transparent media with adjustable axial length and location. Opt. Express 18, 24688–24697 (2010)
117. Feng, Q., Moloney, J.V., Newell, A.C., Wright, E.M., Cook, K., Kennedy, P.K., Hammer, D.X., Rockwell, B.A., Thompson, C.R.: Theory and simulation on the threshold of water breakdown induced by focused ultrashort pulses. IEEE J. Quantum Electr. 33, 127–137 (1997)